citrOgen: a synthesis-free polysaccharide and protein antigen-presentation to antibody-induction platform

Short title

A *Citrobacter rodentium*-based antigen presentation platform

Joshua L C Wong[#,*], Julia Sanchez-Garrido[#], Jaie Rattle, Jonathan Bradshaw, Vishwas Mishra and Gad Frankel[*]

Department of Life Sciences, Imperial College London, SW7 2AZ, UK

[#]These authors contributed equally to this work

[*]For correspondence:

Electronic mail: joshua.wong@imperial.ac.uk and g.frankel@imperial.ac.uk

Keywords

Antibodies, *Citrobacter rodentium, Klebsiella pneumoniae,* type III secretion system (T3SS), EspO

Abstract

Existing technologies employed to generate antibodies against bacterial polysaccharides and proteins rely on the availability of purified or synthetic antigens. Here we present a genetics-based platform that utilises *Citrobacter rodentium* (CR), an enteric mouse pathogen, to both produce and present complex heterologous polysaccharides and protein antigen complexes during natural infection. As proof of concept, we use lipopolysaccharides (O), capsular polysaccharides (K) and type 3 fimbrial (T3F) antigens expressed by the WHO critical priority pathogens *Klebsiella pneumoniae* (KP) and *Escherichia coli* (EC). Following one infection cycle (28 days) CR induces specific IgG antibodies against KPO1, ECO25b, KPK2 and KPT3F. We demonstrate that the antibodies are functional in downstream applications including protection against pathogenic KP challenge, KP capsular serotyping and KP biofilm inhibition. Whilst KP and EC antigens were used as prototypical examples, this modular platform is now readily adaptable to generate antibodies against diverse polysaccharide and protein antigens, with basic science, public health and therapeutic applications.

Introduction

The specificity of antibody/antigen (Ab/Ag) binding has been widely leveraged in science, biotechnology, and medicine. Both polyclonal (pAb) and monoclonal (mAb) antibodies are routinely employed across these disciplines and have shaped the face of the modern practice. There is, therefore, significant value in expanding the technologies available to generate new Abs that bind specific Ags of interest.

Abs are employed widely in the field of infectious disease with both diagnostic and, more recently, therapeutic applications. One key use in diagnostics is bacterial serotyping, which has played important roles in pathogen epidemiology. Therapeutic Abs are licensed for both the prevention and treatment of viral and bacterial infections in humans. Palivizumab, a humanised monoclonal IgG Ab that binds Respiratory Syncytial Virus, was the first mAb licensed for the prophylaxis of infectious disease in 1998[1]. Bezlotoxumab, a mAb against the enteric pathogen *C. difficile*, the sole mAb licensed in bacterial disease, was licensed in 2016 for the secondary prevention of *C. difficile* colitis [2]. More recently, during the SARS-CoV-2 pandemic both pAb administration (convalescent sera)[3] and mAbs against spike protein (e.g. bamlanivimab, etesevimab, casirivimab and imdevimab)[4] were used in the prevention and treatment of COVID-19 disease.

We currently have limited therapeutic options to combat the antimicrobial resistance (AMR) pandemic with both anti-bacterial Abs (□-bAbs) and vaccines representing promising modalities to tackle this contemporary threat. Vaccines rely on inducing an enduring memory response through the immunisation of naïve populations with target bacterial Ags. This allows adaptive host immunity to briskly reactivate upon subsequent pathogen exposure, clearing infection and reducing disease severity. In the case of extracellular bacteria, the effector arm of this response is centrally mediated by Abs. In contrast, □-bAb therapeutics are produced *in vitro* and administered to patients as prophylaxis or in treatment settings. Uniquely, Fc-enhanced effector functions can be molecularly introduced to □-bAbs that prolong intravascular half-life or promote hexamerisation and

40 complement-mediated cytotoxicity[5,6]. There are merits and disadvantages to both approaches, for
41 example, whilst -bAb administration ensures that the effector arm of the host response is delivered
42 directly to the patient, it fails to induce immunological memory. However, memory responses are
43 often blunted in the high-risk populations that would benefit most from vaccination, such as the
44 elderly[7]. As such, both approaches are being actively pursued and could be used in combination or to
45 target different populations.

46 In target-specific -bAb campaigns Abs that bind predetermined Ags are generated and selected for
47 downstream applications. Target choice can be informed *a priori* by pathogen epidemiology and
48 genomics, selecting bacterial Ags that are both widespread and conserved across a bacterial species.
49 Ags representing virulence determinants can also be selectively targeted as Ab-binding has the
50 potential to functionally disrupt pathogenic mechanisms[8]. The immunisation of experimental animals
51 or human subjects is a common method to generate target-specific Abs. This results in sera
52 containing pAb secreted from reactive B-cells. These cells can be immortalised or Ab-encoding
53 regions subcloned to produce mAbs *in vitro*. Irrespective of host species or Ag, the generation of
54 such responses is fundamentally reliant on a sufficient source of conformationally correct
55 immunogen. Generating these immunogens represents a key bottleneck in both target-specific Ab
56 generation[9] and vaccine development.

57 Polysaccharide Ags are diverse and typically composed of variable sugar subunits, each covalently
58 connected in the correct order by specific glycosidic links. These linkages can be linear or include
59 branching arrangements that determine the final polysaccharide structure. In isolation,
60 polysaccharides typically require carrier protein glycoconjugation to generate formulations that are
61 sufficiently immunogenic[9]. Production of sufficient quantities of protein Ags, which are typically
62 affinity purified following *de novo* synthesis in cells, is largely restricted to protein monomers and not
63 applicable to multiprotein complexes. The correct formation of the latter not only requires the
64 presence of chaperones and signal sequences, directing subunit assembly in the correct subcellular
65 space, but also necessitates conformationally correct monomers to interact with each other in the

66 correct stochiometric ratio. Bacterial genomes have compartmentalised the genes required to
67 synthesise both polysaccharide and multimeric protein Ags into operons, providing cloneable linear
68 DNA fragments that we exploit in the development of the technology we describe here.

69 *Citrobacter rodentium* (CR) causes colitis in mice with an infection strategy mirroring the human
70 pathogen Enteropathogenic *Escherichia coli* (EPEC). CR attaches intimately to intestinal epithelial
71 cells (IECs) forming attaching and effacing lesions and actin-rich pedestal-like structures, a
72 prerequisite for productive infection and colitis[10]. A major virulence factor enabling CR infection is
73 the type 3 secretion system (T3SS)[11] which translocates 31 effector proteins into IECs, facilitating CR
74 adherence and proliferation[12]. The resolution of CR infection coincides with the onset of IgG
75 secretion[13,14]. However, until this adaptive immune response clears the infection, CR maintains high
76 mucosal-associated burdens, inducing significant local inflammation with associated immune cell
77 recruitment[12]. We hypothesised that this natural host-pathogen context represents an evolutionarily
78 pre-optimised environment to present alternative (heterologous) Ags to the mouse host, thereby
79 generating mature target-specific Ab responses. This hypothesis forms the basis of our platform
80 which we term citrOgen.

81 Heterologous Ag delivery employing alternative bacterial chassis has been evaluated in previous
82 studies and largely focussed on live attenuated vaccine candidates. Common candidates include
83 *Salmonella typhimurium* and *Shigella spp*, where heterologous Ag expression aims to broaden the
84 vaccines range to now include pathogens beyond the attenuated candidate itself[15–17]. This field has
85 been hampered by the low stability of heterologous Ags *in vivo* and failure to induce protective
86 responses. Indeed, when the licensed live-attenuated *Salmonella typhi* vaccine strain Ty21a
87 expressing *Shigella sonnei* O2a Ag was administered to human subjects, only 19-27% (n=121
88 participants) had detectable *S. sonnei* IgG responses[18]. A subgroup of participants and controls then
89 underwent *S. sonnei* challenge and clinical shigellosis developed at the same rate in both groups,
90 providing no evidence of protection or amelioration of disease.

91 citrOgen is a flexible and modular *in vivo* Ag presentation platform co-opting CR to present
92 heterologous Ags. It represents a single unifying genetics-based system that can be used to generate
93 functional target-specific -bAb responses to divergent major Ag subtypes in mice. We selected four
94 structurally diverse and validated Ags from the WHO critical priority pathogens *Klebsiella*
95 *pneumoniae* (KP) and *E. coli* (EC) to test the platform [19]. The choice includes two surface
96 polysaccharide families, lipopolysaccharide (LPS – KP O1 & EC O25b) and capsular polysaccharide
97 (CPS – KP K2) and a protein complex, type 3 fimbriae (KP T3F). Substituting the endogenous CR O152
98 LPS O-Ag with KP O1 resulted in lower gut colonisation, which we overcome by overexpressing the
99 CR T3SS effector EspO. Functionally, EspO-augmented -KP O1 Ab responses potently protected mice
100 from sepsis-induced organ failure following KP challenge. Furthermore, we were able to rapidly
101 modify CR to express EC O25b eliciting specific -EC O25b IgG responses after a single infection cycle
102 (28 days) in mice. We then successfully generated -CPS Abs, which we employed to serotype a
103 diverse KP collection of 100 clinical isolates. Finally, we demonstrate citrOgen's ability to raise Abs to
104 a large cell surface filamentous structure, KP T3F, the regulated expression of which we designed to
105 coincide with CR attachment to host epithelia. These -KP T3F Abs effectively blocked T3F-mediated
106 KP biofilm formation. Together these results demonstrate the ability to rapidly generate functional
107 target-specific Abs against a broad range of major bacterial Ags.

108

109 **Results**

110 **Heterologous KP O1 O-antigen expression causes an in vivo colonisation defect**

111 Our goal was to express diverse heterologous Ags in CR to generate target-specific Abs in mice. The
112 *rfb* locus typically encodes all the genes required for O-Ag synthesis and export in Gram-negative
113 bacteria[20]. An exception is the KP O1 Ag, where *rfb*-derived O2 Ag is modified by the
114 glycosyltransferase activity of two enzymes, WbbY and WbbZ, which are encoded at a distinct
115 chromosomal position[21]. Moreover, KP employs an ABC-transporter instead of the more common
116 *wzy*-dependent O-Ag export process used by CR_{WT}[22].

117 We started by identifying the *rfb* locus in CR_{WT}, which is encoded on the reverse strand and flanked
118 by *galF* (5') and *gnd* (3') genes (Fig 1A). We used *in silico* serotyping to confirm that CR_{WT} encodes an
119 *E. coli*-like O152 Ag[23]. The endogenous O152 genes were replaced with those comprising the KP O2a
120 *rfb* locus (cloned en bloc) by homologous recombination and the *wbbYZ* gene cluster inserted into
121 the CR genome by Tn7 transposon mutagenesis (Fig 1A)[24]. Tn7 inserts at a neutral insertion site,
122 downstream of the *glmS* site *(attTn7* site) and we have already used this approach to successfully
123 express multiple different cargos in vivo[25]. This strain, CR_{KPO1}, contains all the genetic determinants
124 required to synthesise and export KP O1 Ag, albeit using a non-native ABC-transporter export
125 pathway. We did not modify the CR gene products that synthesise lipid A or core oligosaccharide (Fig
126 1B) and, therefore, CR_{KPO1} is predicted to produce a hybrid LPS molecule; the endogenous CR Raetz
127 pathway and CR *rfa* locus producing lipid A and core regions, respectively, with KP O1 Ag attached to
128 the native CR lipooligosaccharide scaffold (Fig 1B). We purified LPS from KP_{WT}, CR_{WT} and CR_{KPO1} and
129 confirmed the presence of a substituted O-antigen CR_{KPO1} by silver stain, with a banding pattern
130 distinct from CR_{WT} and similar to KP_{WT} (Supplementary Fig 1A). The specificity of O-antigen
131 substitution was confirmed Western blot. As anticipated α-O152 pAb sera recognised CR_{WT} but was
132 not reactive against KP_{WT} and CR_{KPO1} (Fig 1C). We then used an α-KP O1 mAb (C13)[26], which bound to
133 both KP_{WT} and CR_{KPO1}, confirming heterologous O-antigen expression in CR. The homologous
134 recombination vector employed to substitute the KP O2 locus was designed to include the

135 endogenous 5' CR promoter, ensuring that future O-antigen locus substitutions can be achieved by
136 using the same vector, simply modified with O-antigen genes of choice.

137 We tested if replacing CR O152 with KP O1 affected infectivity *in vitro* and confirmed that CR_{KPO1}, like
138 $CR_{WT,}$ induced actin-rich pedestal formation following the infection of mouse fibroblasts cells.
139 Furthermore, detectable KP O1 Ag expression was restricted to CR_{KPO1} (Supplementary Fig 1B). We
140 therefore proceeded to infect CD-1 mice with 10^9 colony forming units (CFUs) of CR_{WT} or CR_{KPO1} by
141 oral gavage (Fig 1D). At 8 days post infection (dpi), when stool CR shedding peaks, faecal CR_{KPO1} CFU
142 counts were significantly lower than CR_{WT} (Fig 1D). Staining of colonic sections revealed that whilst
143 CR_{KPO1} maintained heterologous KP O1 expression *in vivo,* there were substantially fewer adhered
144 bacteria compared to CR_{WT} (Fig. 1E, Supplementary Figure 1C). These data indicated an *in vivo*
145 colonisation defect imposed by heterologous Ag expression that needed to be addressed to develop
146 an optimal platform.

147 **EspO overexpression restores CR_{KPO1} colonisation**

148 A mutant in the *Shigella flexneri* T3SS effector *ospE*, a homologue of the CR effector *espO*, results in a
149 colonisation defect in a guinea pig gut infection model, as OspE suppresses epithelial detachment[27].
150 We therefore hypothesised that over expression of EspO would promote greater bacterial
151 attachment to IECs during infection. Indeed, while deletion of *espO* in CR_{WT} showed a tendency
152 towards decreased proportion of CR-associated IECs, overexpression of EspO increased the
153 proportion from 14.6% to 22.9% (Supplementary Fig 2A-C). We then overexpressed EspO in CR_{KPO1}
154 (CR_{KPO1}+p*espO*) and infected CD-1 mice; infections with CR_{WT} and CR_{KPO1} were used as controls.
155 Enumeration of faecal CFUs now revealed no difference between the faecal CFUs between CR_{WT} and
156 CR_{KPO1}+p*espO* at 8 dpi (Fig 2A). Staining of colonic sections demonstrated higher levels of
157 CR_{KPO1}+p*espO* adhesion to the epithelia compared to CR_{KPO1}, which maintained heterologous KP O1
158 expression *in vivo* (Fig 2B).

159

160 **CR_{KPO1}+p*espO* infection elicits KP O1 specific IgG antibodies**

161 We inoculated mice with CR_{KPO1}+p*espO* and CR_{WT} by oral gavage. After CR clearance (c. 28 dpi) we
162 collected blood and assessed α-KP_{WT} IgG antibody titres by enzyme-linked immunosorbent assay
163 (ELISA), using a capture plate coated with heat-killed KP_{WT}. While control CR_{WT} mice sera had
164 negligible α-KP_{WT} IgG binding, this increased significantly in sera from CR_{KPO1}+p*espO*-infected mice,
165 indicating that we had successfully raised α-KP_{WT} Abs (Fig. 2C). To confirm the specificity of the Ab
166 response we used an isogenic rough (absent O-antigen) KP mutant, $KP_{\Delta rfb}$, and assessed binding to
167 live bacteria by flow cytometry (Fig. 2D). Consistent with the ELISA data, sera from CR_{WT}-infected
168 mice bound to neither KP_{WT} nor $KP_{\Delta rfb}$. However, sera from CR_{KPO1}+p*espO*-infected mice bound
169 specifically to KP_{WT} and not $KP_{\Delta rfb}$, confirming the presence of α-KP O1 Abs (Fig 2D, Supplementary
170 Fig 2D). We then assessed the pattern of binding to KP_{WT} by immunofluorescence (IF) microscopy (Fig
171 2E). This confirmed the same pattern of binding of CR_{KPO1}+p*espO* sera and the reference α-KP O1 Ab
172 C13. No detectable signal was observed in sera from CR_{WT}-infected mice.

173 **Anti-KPO1 IgG Abs are functionally protective against KP pulmonary challenge**

174 We next tested the functionality of the CR_{KPO1}+p*espO*-induced α-KP O1 pAbs by lung challenge with
175 KP_{WT}. Mice that had been infected and cleared CR_{KPO1}+p*espO* were intubated and administered 500
176 CFU of KP_{WT} directly into the lungs. In preliminary experiments with CD-1 mice this KP_{WT} inoculum
177 was found to result in a progressive increase in KP CFUs in the lungs and blood resulting in a severe
178 disease phenotype at 72 h post infection (hpi) (Supplementary Fig 3 A-C). Mice that had been
179 infected by and subsequently cleared CR_{WT} were also challenged as controls. We evaluated infection
180 outcomes by assessing KP_{WT} replication and protection against host organ failure employing markers
181 of haematological, lung and renal injury in line with international consensus[28,29]. At 72 hpi KP_{WT}
182 burdens in the lungs of CR_{WT}-preinfected mice reached a median of c. 10^9 CFUs (Fig 3A). In contrast,
183 CR_{KPO1}+p*espO*-preinfected mice had significantly reduced lung CFUs with KP_{WT} only detectable in the
184 lungs of 30% (5/14) of mice. KP bacteraemia was absent in all CR_{KPO1}+p*espO*-preinfected mice in
185 comparison to 69% (9/13) of CR_{WT}-preinfected control mice (Fig 3B).

186 We then assessed if the reduction of KP_{WT} burden translated into a positive effect on host physiology.
187 Only 3 mice (20%, 3/15) in the CR_{KPO1}+p*espO*-preinfected group lost more than 10% of their starting
188 weight when challenged with KP_{WT}, whereas all mice in the CR_{WT}-preinfected group lost weight after
189 KP challenge with 86% (12/14) losing more than 10% of their starting weight (Fig 3C). Total white cell
190 counts, lymphocyte counts and platelets in the blood demonstrated significantly positive
191 improvements in CR_{KPO1}+p*espO*-preinfected mice compared to CR_{WT}-preinfected animals (Fig 3D-F).
192 Specifically, the extent of sepsis-induced leucopaenia, lymphopaenia and thrombocytopaenia were
193 abrogated by the CR_{KPO1}+p*espO* preinfection, while the number of neutrophils did not change
194 between the mouse groups (Fig 3G). Moreover, the positive acute phase reactants (APR) Serum
195 amyloid A and C-reactive protein were significantly lower in CR_{KPO1}+p*espO*-preinfected mice
196 compared CR_{WT}-preinfected animals (Fig 3H&I). This beneficial modulation in APRs translated into
197 higher levels of the negatively regulated APR, albumin, in CR_{KPO1}+p*espO* preinfected mice (Fig 3J).

198 We then used three markers to assess lung injury: IL1β and myeloperoxidase (MPO) in lung
199 homogenate and surfactant protein D (SPD) levels in the serum[28]. This revealed that CR_{KPO1}+p*espO*
200 preinfection resulted in significant reductions in IL1β and SPD levels compared to CR_{WT} preinfection,
201 indicating reduced lung inflammation and improved maintenance of the alveolar capillary barrier
202 respectively (Fig 3K&L). Preinfection with CR_{KPO1}+p*espO* also resulted in significantly reduced
203 neutrophilic alveolitis, evidenced by reduced lung MPO levels compared to CR_{WT}-preinfected mice
204 (Fig 3M). Finally, we assessed acute kidney injury by measuring serum creatinine and cystatin C
205 levels. While high levels of creatinine and cystatin C were found in KP_{WT} challenged CR_{WT}-preinfected
206 mice, improvements in both excretory renal function markers were seen in CR_{KPO1}+p*espO*-preinfected
207 mice (Fig 3N&O). These data indicate that -KP O1 Abs raised by citrOgen were protective against KP
208 challenge, restricting both bacterial replication and dissemination, and preventing KP sepsis-induced
209 organ failure.

210 **citroGen can rapidly be adapted to present alternative O-antigens**

211 Having overcome the fitness cost imposed by heterologous O Ag expression in CR and demonstrated
212 functional responses we wanted to further test the platform's modular nature and efficiency. To that
213 end, we selected *E. coli* O25b Ag (EC O25b), frequently encoded by ESBL-producing ST131 *E. coli*
214 strains (EC958 representing the prototype[30]) and used our vector system to generate CR_{ECO25b} (Figure
215 4A). O25b Ag was selected for two reasons, firstly, it is expressed an alternative WHO critical priority
216 pathogen and secondly, it is exported by the most common wzy-dependent export pathway. The
217 additional gene, *wzz*, which lies outside the *rfb* locus, is a chain length determinant in wzy-
218 dependent systems; we did not replace this and opted to keep the native CR_{WT}-encoded variant. We
219 confirmed specific O25b expression by agglutination, using reference □-O25b pAb sera, which
220 agglutinated EC958 and CR_{ECO25b} but not $CR_{WT.}$ (Fig 4B). Silver staining of LPS preparations confirmed
221 the presence of O Ag in CR_{ECO25b}, which now runs at a higher molecular weight, as dictated by the
222 novel wzz(CR)/wzy(EC958) interaction (Supplementary Fig 4). Mice were orally infected with
223 CR_{ECO25b}+p*espO* and at 8 dpi no colonisation defect was observed compared to CR_{WT} (Fig4C). Blood
224 was collected from mice after CR clearance and sera used in an ELISA against EC958 and an isogenic
225 rough mutant ($EC958_{\Delta rfb}$). Absent Ab responses were detected from CR_{WT}-infected mice against either
226 EC958 or $EC958_{\Delta rfb}$. However, sera from mice infected with CR_{ECO25b}+p*espO* specifically reacted to
227 EC958 with absent binding to $EC958_{\Delta rfb}$ (Fig 4D). This specificity confirmed that citrOgen can be used
228 against additional O Ags, irrespective of export pathway. Moreover, it confirms that Ag selection to
229 antibody production is achievable in c. 35 days.

230 **citroGen presentation of heterologous KP capsular polysaccharide antigen**

231 We next explore expanding the citrOgen platform to generate □-CPS Abs. KP_{WT} produces K2 CPS,
232 encoded by a c. 22Kb K2 *cps* locus, lying immediately upstream of the *rfb* locus in the KP_{WT} genome.
233 As upstream of the CR O152 *rfb* locus lie the genes involved in synthesis and export of the
234 extracellular polysaccharide colanic acid (Fig. 5A), we replaced the CR_{WT} genes between *ROD21991*
235 and *galF* (c. 24kb) with the KP KL2 operon from *wzi* to *manB* by homologous recombination,
236 generating strain CR_{KPK2}+p*espO* (Fig. 5A). We chose this insertion site as we anticipate that it will

237 tolerate other *cps* locus insertions in future applications of this technology. This established vector
238 can be used as the template together with *cps* locus of choice (e.g. KP *cps* loci vary from 10-30kb and
239 include internal promoters[31]).

240 We infected mouse fibroblasts to evaluate if the expression K2 capsule impacted on CR T3SS
241 functionality. CR_{KPK2} formed actin-rich pedestals and heterologous K2 expression was confirmed by
242 staining with reference K2 antiserum (Supplementary Fig 5A). This suggests that the K2 capsule does
243 not obstruct the T3SS needle, likely due to the fact that it is extended by a long EspA filament[32]. We
244 confirmed that EspO overexpression was required for optimal colonisation in the context of
245 heterologous CPS expression, as mice orally infected with CR_{KPK2} colonised at a lower level compared
246 to CR_{WT} at 8dpi (Supplementary Fig. 5B). We then proceeded to infect CD-1 mice with CR_{KPK2}+p*espO,*
247 or CR_{WT} as a control, which were shed at comparable levels (Fig 5B). Following CR_{KPK2}+p*espO* and CR_{WT}
248 clearance, we collected blood samples and α-KP IgG levels were assessed by ELISA, using KP_{WT} and an
249 acapsular *wcaJ* mutant, $KP_{\Delta wcaJ}$. No binding to either KP_{WT} or $KP_{\Delta wcaJ}$ was observed with sera from
250 CR_{WT}-infected mice. In contrast, sera from mice infected with CR_{KPK2}+p*espO* bound to KP_{WT} but not to
251 $KP_{\Delta wcaJ}$ (Fig 5C). This indicated that KP K2 was successfully presented by the citrOgen platform *in vivo*
252 and that α-KP IgG was specifically raised against the heterologous KP K2 antigen.

253 KP strains demonstrate broad diversity in CPS Ags with over 147 described to date in circulating
254 strains[31]. However, despite their key role in virulence and frequent use in genome-based
255 epidemiology, no reference antisera are currently being produced for *in vitro* applications. We used
256 sera derived from CR_{KPK2}+p*espO* infection, together with a reference K2 antiserum as a control, to
257 stain KP_{WT}. No detectable binding was seen in sera from CR_{WT}-infected mice. In contrast, binding was
258 seen when KP_{WT} was stained with the CR_{KPK2}+p*espO* sera, which phenocopied the pattern of binding
259 seen with the reference K2 antiserum (Fig. 5D). Together with the ELISA results, this provides strong
260 evidence for specific heterologous α-KP K2 Abs induced by CR_{KPK2}+p*espO* infection.

261 **KP serotyping using the citrOgen KP K2 sera**

262 We next tested if the citrOgen KP K2 sera could be used for serotyping. To this end, we used a
263 publicly available collection of 100 KP isolates, representing 54 distinct CPS types determined by
264 genomic analysis[33]. We incubated the strains with citrOgen KP K2 sera and analysed binding by flow
265 cytometry (Fig 5E, Supplementary Fig. 5C). We included KP_{WT} and $KP_{\Delta wcaJ}$ as controls and measured
266 the median fluorescence intensity (MFI) across the collection. The citrOgen KP K2 sera specifically
267 bound KL2 isolates and KP_{WT} with minimal cross reactivity and absent binding to $KP_{\Delta wcaJ}$. This binding
268 was comparable to that observed when staining the KL2 strains with our reference K2 antiserum (Fig
269 5E, Supplementary Fig. 5D). To confirm the KL assignments, we selected 9 isolates for IF with the
270 reference K2 antisera (Fig 5F). We observed a pattern of binding consistent with capsule in the KL2
271 strain but not the surrounding non-KL2 strains. We concluded that the citrOgen KP K2 sera can be
272 used for serotyping and validated the collection's KL2 assignments.

273 **citroGen presentation of heterologous protein complex antigens**

274 We next assessed the utility of citrOgen in generating Abs against heterologous proteins, using the
275 well-conserved KP T3F as a model protein complex[34]. T3F are a KP virulence factor that mediate
276 binding to abiotic surfaces (such as plastic and glass) and are involved in the first steps of biofilm
277 formation. The major T3F subunit is MrkA which together with MrkD (adhesin tip) and MrkF
278 (unknown function) are externalised via a β-barrel transmembrane usher protein, MrkC, and
279 assemble into T3F on the KP cell surface (reviewed in Murphy et al. 2012[35]). In the periplasm a
280 chaperone, MrkB, binds MrkA to prevent ectopic pilin polymerisation. Therefore, MrkABCDF, are all
281 required for T3F biogenesis. T3F expression is tightly regulated in KP by an adjacent operon (*mrkHIJ*)
282 via the second messenger cyclic-di GMP[36]. To coordinate expression of the T3F with CR attachment
283 to IECs *in vivo,* we constructed a citrOgen strain in which *mrkABCDF* (excluding *mrkHIJ*) was driven by
284 the promoter of the T3SS effector *map* (CR_{T3F})[37]. The recombinant operon was inserted into the CR
285 *glmS* site (Fig 6A). We perceived two significant advantages of this strategy, firstly, maximising T3F
286 expression during intimate attachment to host cells and secondly to limit the metabolic burden of
287 T3F expression in CR. To confirm accurate gene regulation, we quantified *mrkA* transcript levels in

288 T3SS-suppressing (LB media, static growth) and T3SS-inducing (DMEM, static growth) conditions
289 (Supplementary Fig 6A)[38]. qRT-PCR analysis demonstrated low *mrkA* transcripts from CR_{T3F}+*pespO*
290 grown in LB which increased significantly in DMEM (Fig 6B), a change also observed for the
291 endogenous *map* gene used as a positive control (Supplementary Fig. 6A). No *mrkA* transcripts were
292 detected in the CR_{WT} negative control. We then confirmed that CR_{T3F} formed actin-rich pedestals *in*
293 *vitro* and expressed KP T3F by staining with an ⍰-MrkA pAb (Supplementary Figure 6B). Finally, we
294 tested if T3F conferred CR_{T3F} the ability to adhere to glass under T3SS inducing conditions. This
295 revealed a stark increase in the number of adhered CR_{T3F} observed on glass coverslips compared to
296 CR_{WT} when both were grown statically in DMEM, indicating functional heterologous T3F expression
297 (Fig 6C). Whilst this vector was designed to insert and provide stringent control of T3F expression it
298 can be readily be used for the expression of other operons encoding mono/multimeric protein Ags to
299 facilitate future iterations of this technology.

300 We started by confirming if EspO overexpression was required in the context of complex protein Ag
301 expression and infected mice with CR_{T3F} and CR_{WT}. A similar colonisation defect was evident at 8dpi
302 that we had encountered when KP O1 or KP K2 were expressed in CR_{WT} (Supplementary Fig. 6C). We
303 next used oral gavage to infect CD-1 mice with CR_{T3F}+p*espO*, which colonised similarly to CR_{WT} at 8
304 dpi (Fig 6D). We used the sera collected from mice who had cleared the infection for ELISA, with
305 plates coated with heat killed KP_{WT} and $KP_{\Delta mrkA\text{-}F}$, a deletion mutant in the T3F structural genes. Sera
306 collected from the control CR_{WT}-infected mice were not reactive against KP_{WT} or the isogenic mutant
307 (Fig 6E). Conversely, sera from CR_{T3F}+*pespO* -infected mice bound $KP_{WT,}$ with absent binding to
308 $KP_{\Delta mrkA\text{-}F.}$ This data confirmed the ⍰-KP IgG antibodies were directed towards T3F. Using pooled sera
309 from the CR_{T3F}+*pespO* infected mice to stain KP_{WT} revealed a binding pattern that matched that of
310 the reference ⍰-MrkA pAb (Fig 6F). As T3F mediate attachment to abiotic surfaces and biofilm
311 formation, we then tested if the sera from could prevent KP_{WT} attachment. We first pre-adsorbed the
312 sera from CR_{T3F}+p*espO*- and CR_{WT}-infected mice against PFA-fixed CR_{WT} to remove ⍰-CR Abs (10x 24h
313 adsorption cycles against fresh PFA-fixed CR_{WT}) (Supplementary Fig. 6D). This resulted in sera that

314 negligibly bound CR_{WT} (Supplementary Fig. 6E&F). We preincubated these two preadsorbed sera,
315 which had equivalent concentrations of total IgG (Supplementary Fig 6G), with KP_{WT} expressing sfGFP
316 and measured attachment after static growth at 37°C. Sera from CR_{T3F}+p*espO*-infected mice resulted
317 in 3-fold reduction in KP attachment compared to sera from CR_{WT}-infected mice (Fig. 6G&H). These
318 data demonstrate the generation of ⍰-KP T3F Abs that functionally inhibit surface attachment, the
319 first step in KP biofilm formation.

320 **Discussion**

321 LPS, CPS and proteins are common bacterial targets where generating specific Abs is desirable.
322 Whilst techniques already exist to generate such target-specific Abs, individually tailored and time-
323 consuming approaches are required to prepare the Ags. Here, instead, we co-opt the mouse
324 pathogen CR for this purpose and combine the steps of Ag preparation and immunisation into a
325 single platform that both expresses heterologous Ags and presents them continuously, in their native
326 conformation, to the host over the entire infection cycle (Figure 7). This was achieved by
327 recombination-based genome editing in which whole operons were cloned from KP and inserted or
328 substituted into the CR; thus, all genetically encoded components are inherently included, ensuring
329 that Ag assembly takes place in a fashion mirroring the pathogen of choice. It should be noted that,
330 whilst we achieve this for four diverse Ags, they all come from Gram-negative *Enterobacterales*,
331 which will have favoured our approach. Nevertheless, we were able to achieve specific and
332 functional Ab responses for LPS, CPS and a large protein complex. If we consider the latest iteration
333 of the WHO Bacterial Priority Pathogens List[19] then three out of four critical pathogens are Gram-
334 negatives, indicating the clear and present danger posed by this group of bacterial threats. The data
335 we present already supports using citrOgen for bacterial Ag targets in these key organisms. We
336 anticipate that further modifications will be required to synthesise and present Gram-positive
337 bacterial Ags. As well as the ability to present complex polysaccharide structures and
338 multicomponent protein Ags in their native location and configuration, one key advantage of
339 citrOgen is time (Fig 7). In this work we have already validated substitution/insertion sites and
340 generated the appropriate genome editing vectors. Changing the inserts encoded by these vectors
341 (to alternative LPS, CPS and protein Ags) is routine and together with subsequent CR genome editing
342 can be achieved over a period of days. Whilst we cloned sequences directly from EC and KP DNA we
343 propose that this technology could also be applied to generate diagnostic or therapeutic Abs in an
344 outbreak scenario. The now routine use of *de novo* gene synthesis would enable us to engineer
345 strains based on early sequencing data alone. This would allow us to use this platform to generate

346 pAb sera in as little as 28 days- a complete CR infection cycle in mice. In more controlled settings we
347 envisage generating citrOgen strains encoding multiple Ags simultaneously. Ethically, this reduces the
348 number of experimental animals for use in research and development and would permit multiple
349 target-specific Ab responses to be obtained following a single infection.

350 We overcame two major obstacles to develop a viable platform for broader applicability. The first
351 was the potential fitness cost imposed by heterologous Ag expression. Indeed, we observed lower
352 gut colonisation in $CR_{KPO1,}$ CR_{KPK2} and CR_{T3F} compared to CR_{WT}, a defect that only becomes evident
353 under the pressure of the host-pathogen-microbiome environment. We overcame this obstacle by
354 overexpressing the T3SS effector EspO, which promotes IEC attachment and mucosal colonisation.
355 The second was the metabolic cost to CR of dysregulated heterologous protein expression which we
356 overcame by placing expression under the control of the endogenous CR promoter for the *map* gene.
357 This restricts heterologous protein expression to T3SS-inducing conditions and promotes
358 presentation at host mucosal surfaces, a strategy that can be used for the expression of any
359 heterologous protein, where expression needs to be tightly controlled and/or where regulatory
360 genes are absent in CR. Further modifications for expression can now easily be implemented given
361 the rich genetic toolset provided here or that already available for *E. coli,* a close relative of CR, which
362 shares similar genetic tractability.

363 In the case of KP O1 Ag we combined citrOgen with subsequent KP lung challenge, which allowed us
364 to quantitively evaluate protection from organ failure conferred by the □-bAb response to this Ag (Fig
365 3). Given the current lack of correlates of protection for bacterial infections we propose that citrOgen
366 strains may represent an efficient tool to evaluate future proposed Ags. Strains engineered to
367 express heterologous Ags (singly or in combination) can be used to evaluate Ab responses following a
368 CR infection cycle. In the same cohort of mice, subsequent pathogenic challenge can then evaluate
369 the protection conferred by the response. Expanding the translational applicability of current priority
370 bacterial infection models would significantly enhance the data we could achieve in this approach.

371 CR infections are host restricted to mice, conferring platform safety and preventing infection risk to
372 humans. This is especially important as future citrOgen strains could include additional virulence
373 factors as Ags for Ab generation. We currently use the citrOgen platform in conventional mice
374 generating murine immunoglobulins. Advances in molecular genetics have enabled the generation of
375 'humanised' Abs initially raised in non-human species and could be applied to the current iteration of
376 the platform[39]. This improves IgG tolerability and durability when administered to human patients
377 largely by reducing the immunogenicity provoked by non-human Ig regions. Furthermore, extensive
378 work in the field of mouse genetics has enabled the generation of fully human Abs in transgenic
379 animals[40]. Combining these transgenic mice with citrOgen strain infection would result in human Ig
380 induction in one CR infection cycle (Fig 7). Existing downstream workflows, such as hybridoma
381 generation or IgG loci subcloning are already well defined and employed to produce mAbs from B-
382 cells derived from these mice. Whilst our antibiotic treatment options are rapidly diminishing the
383 application of this technology may alleviate future infectious diseases deaths by generating new Ab-
384 based diagnostic tools and therapeutics.

385 **Figure Legends**
386
387 **Figure 1. Heterologous KP O1 O-antigen expression causes and *in vivo* colonisation defect.**
388
389 A. The *rfb locus* in CR_{WT} encodes a O152-like *E. coli* O-antigen locus located between *galF* and *gnd*. In
390 CR_{KPO1} the CR_{WT} *rfb* locus was substituted with the genes encoding KP O2a O-antigen and *wbbYZ*
391 (converted KP O2a to KP O1v1) inserted at the 3' *glmS* site.
392
393 B. CR_{KPO1} expresses a hybrid lipopolysaccharide molecule with native CR lipid A and core
394 lipooligosaccharide linked to KP O1 Ag. The western blot is representative of 2 biological repeats.
395
396 C. Western blot confirmation of heterologous KP O1 Ag in CR_{KPO1} performed on purified LPS
397 preparations. α-O152 Ab are immunoreactive with CR_{WT} but not KP_{WT} or CR_{KPO1} whereas α-KP O1 mAb
398 (C13) is immunoreactive with both KP_{WT} and CR_{KPO1}.
399
400 D. At 8 dpi following oral gavage, faecal CFUs are significantly lower in CR_{KPO1} compared with CR_{WT}.
401 n=10 mice per group, 2 biological repeats. Central tendency: median. Mann-Whitney test. **,
402 $p<0.01$. GoF, gram of faeces.
403
404 E. Colonic histology was taken 8 dpi and stained for CR, KP O1 Ag and DAPI staining used as a
405 structural marker. CR_{WT} is observed confluently adhering to the luminal surface of the colon with no
406 KP O1 Ag expression detectable. Sparse staining for CR_{KPO1} is observed however, where present, KP
407 O1 Ag expression detectable. Scale bar = 200 µm. Images are representative of 3 biological repeats.
408
409 **Figure 2. CR_{KPO1} overexpressing EspO maintains infectivity and induces specific anti-KP O1 Ag IgG**
410 **responses.**
411
412 A. At 8 dpi *espO* overexpression in CR_{KPO1}+p*espO* reverses the colonisation defect observed in CR_{KPO1}
413 restoring colonisation to that of the parental CR_{WT} strain. n=15 mice per group, 3 biological repeats.
414 Central tendency: median. Ordinary one-way ANOVA with Dunnett's multiple comparison.
415
416 B. Colonic histology was taken 8 dpi and stained for CR, KP O1 Ag and DAPI staining used as a
417 structural marker. CR_{KPO1}+p*espO* now confluently adhering to the luminal surface with KP O1 Ag
418 expression detectable and co-localising to CR staining. Sparse staining is observed for CR_{KPO1} with KP
419 O1 Ag expression. Scale bar = 200 µm. Images are representative of 3 biological repeats.
420
421 C. At 30 dpi blood was taken from the tail vein of mice that cleared CR_{WT} and CR_{KPO1}+p*espO*. ELISA,
422 using heat-killed KP_{WT} (expressing KP O1 Ag) revealed α-KP_{WT} IgG in mice following infection with
423 CR_{KPO1} +p*espO* but not CR_{WT} controls. Central tendency: mean. Mann-Whitney test.
424
425 D. Sera from mice was tested for binding to live KP_{WT} and $KP_{\Delta rfb}$. Binding was assessed by flow
426 cytometry and expressed as the percentage of the population positive for mouse IgG (mIgG+ve). Sera
427 from CR_{WT}-infected mice demonstrated absent binding to either KP_{WT} or $KP_{\Delta rfb}$, whereas sera from
428 CR_{KPO1}+p*espO* -infected selectively bound KP_{WT} expressing KP O1 Ag. Central tendency: mean.
429 Unpaired T-test.
430
431 E. Sera from CR_{WT} and CR_{KPO1}+p*espO* -infected mice was used to stain KP_{WT} and image by
432 immunofluorescence microscopy. An α-KP O1 Ag mAb (C13) was used as a positive control for KP O1
433 Ag staining. CR_{WT} derived sera results in no detectable staining of KP_{WT} whereas sera from CR_{KPO1}
434 +p*espO* -infected mice and the control C13 mAb phenocopy each other with membrane-associated
435 staining of KP_{WT}.

436
437 ns=non-significant; *, p<0.5; ****, p<0.0001.
438
439 **Figure 3. Antibodies to KP O1 O-antigen protect against KP pulmonary challenge**.
440
441 Mice that had cleared pre-infection with CR_{WT} and CR_{KPO1}+p*espO* were challenged by intratracheal
442 infection with 500 CFU of KP_{WT}. At 72 hpi we analysed KP replication (A&B) and host-derived severity
443 indicators (C-O). n=15 mice per group (starting) over 3 biological repeats.
444
445 A&B. KP_{WT} replication and bacteraemia are significantly reduced in the lungs (A) and blood (B) of
446 CR_{KPO1}+p*espO*-preinfected mice compared to CR_{WT} controls. Central tendency: median. Mann-
447 Whitney test.
448
449 C. KP_{WT} induces significant weight loss in CR_{WT}-preinfected mice which is reversed in CR_{KPO1}+p*espO*
450 preinfection. Central tendency: mean, error: standard deviation (SD). Mann-Whitney test.
451
452 D-F. Clinical haematological markers of disease severity are significantly improved in CR_{KPO1}+p*espO* -
453 preinfected mice compared to CR_{WT} controls. Total white cell counts (D), lymphocyte counts (E) and
454 platelets counts (F) are significantly lower in CR_{WT}-preinfected controls indicating increased diseases
455 severity. The innate responders, neutrophils (G) are unchanged between the CR_{WT} and CR_{KPO1}+p*espO*
456 preinfected groups. Central tendency: mean, error: SD. Unpaired T-test.
457
458 H-J. The acute phase reactants (Serum amyloid A (H), C-reactive protein (I) and Albumin (J))
459 demonstrate a reduced inflammatory state in CR_{KPO1}+p*espO* -preinfected mice compared to CR_{WT}
460 controls. Central tendency: mean, error: SD. H&J). Mann-Whitney test, I) Unpaired T-test.
461
462 K-M. Acute lung injury markers (lung homogenate IL1β (K), serum surfactant B (L) and lung
463 homogenate myeloperoxidase (M)) are improved by pre-infection with CR_{KPO1}+p*espO* compared to
464 CR_{WT} preinfection. Significant reductions in lung iIL1β, improvement in the alveolar capillary barrier
465 (surfactant protein D) and neutrophilic alveolitis (myeloperoxidase) indicate α-KP O1 Abs protect
466 against lung injury. Central tendency: mean, error: SD. K&M) Mann-Whitney test, L) Unpaired t test.
467
468 N&O. Acute kidney injury and excretory renal failure are reduced in mice preinfected with
469 CR_{KPO1}+p*espO* compared to CR_{WT}. Serum creatinine (N) and serum cystatin C (O) are reduced in KP_{WT}
470 infected mice who have cleared preinfection with CR_{KPO1}+p*espO* compared to CR_{WT}. Central tendency:
471 mean, error: SD. Unpaired t test.
472
473 ns=non-significant; *, p<0.5 **; p<0.01, ***, p<0.001; ****, p<0.0001.
474
475 **Figure 4. Rapid citrOgen modification to present *E. coli* O25b O-antigen**
476
477 A. The CR *rfb locus* editing vector can be rapidly modified to insert the O25b *rfb* locus from EC958
478 (ST131 ESBL producing strain) into the CR genome, generating CR_{ECO25b}.
479
480 B. Agglutination of EC958 and CR_{ECO25b} with polyclonal sera to O25b O-antigen. CR_{WT} forms a tight
481 pellet indicating no agglutination of this strain. In control wells (PBS) all strains form tight pellets in
482 the absence of agglutination.
483
484 C. At 8 dpi following oral gavage, faecal CFUs are not significantly lower in CR_{ECO25b}+p*espO* compared
485 with CR_{WT}. n=10 mice per group, 2 biological repeats. Central tendency: median. Unpaired T-test.
486 GoF, gram of faeces.

487
488 D. At 30 dpi blood was taken from mice that cleared infection with CR_{WT} or CR_{ECO25b}+p*espO*. An ELISA
489 was conducted against heat-killed $EC958_{WT}$ (expressing O25b) and an isogenic rough mutant
490 ($EC958_{\Delta rfb}$). CR_{WT} infected mice had no detectable IgG responses to $EC958_{WT}$ or $EC958_{\Delta rfb}$.
491 CR_{ECO25b}+p*espO* infected mice had IgG responses specifically against $EC958_{WT.}$ n=10 mice per group, 3
492 biological repeats. Central tendency: mean. Unpaired t tests.
493
494 ns=non-significant; ****, p<0.0001.
495
496 **Figure 5. citrOgen derived anti-KP K2 antibodies can be used for serotyping.**
497
498 A. The *cps* in KP_{WT} is c.22kb long with 15 open reading frames. This was inserted into CR_{WT} by
499 substitution of the colanic acid biosynthesis locus generating the strain CR_{KPK2}.
500
501 B. At 8 dpi faecal CR_{KPK2}+p*espO* levels are similar to CR_{WT} . Central tendency: median. n=15 mice per
502 group, 3 biological repeats. Unpaired T-test, ns=non-significant. GoF, gram of faeces.
503
504 C. At 30 dpi blood was taken from mice that cleared infection with CR_{WT} or CR_{KPK2}+p*espO*. An ELISA
505 was conducted against heat-killed KP_{WT} (expressing KP K2) and an isogenic acapsular mutant ($KP_{\Delta wcaJ}$).
506 CR_{WT} infected mice had no detectable IgG responses to KP_{WT} or $KP_{\Delta wcaJ}$. CR_{KPK2}+p*espO* infected mice
507 had IgG responses specifically against $KP_{WT.}$ n=15 mice per group, 3 biological repeats. Central
508 tendency: mean. Mann Whitney test.
509
510 D. Sera from CR_{WT} and CR_{KPK2}+p*espO*-infected mice were used to stain KP_{WT} and image by
511 immunofluorescence microscopy. An α-KP K2 pAb was used as a positive control. CR_{WT} derived sera
512 results in no detectable staining of KP_{WT} whereas sera from CR_{KPK2}+p*espO*-infected mice and the α-KP
513 K2 pAb phenocopy each other with punctate membrane-associated staining of KP_{WT}.
514
515 E. Sera from CR_{KPK2}+p*espO*-infected mice were used to serotype a collection of 100 diverse KP strains
516 with serotypes assigned by genomic analysis. Each box represents one strain with the cps (KL) type
517 described. The boxes are coloured according to the strength of binding by CR_{KPK2}+p*espO*-infected
518 mice sera, which was assessed by flow cytometry. The median fluoresence intensity (MFI) key is
519 shown in the bottom right together with staining of KP_{WT} and $KP_{\Delta wcaJ}$ controls. A box, centred on a KL2
520 isolate is shown.
521
522 F. The strains contained within the highlighted box in (E) were stained with the reference α-KP K2
523 pAb and imaged by immunofluorescence microscopy. The KL2 strain in the centre demonstrate
524 punctate membrane staining in keeping with K2 capsule. The other strains (non-KL2) demonstrate no
525 staining. Bacterial cell membranes were counterstained with FM-4-64 for imaging.
526
527 ns=non-significant; ****, p<0.0001.
528
529 **Figure 6. citrOgen derived anti-KP T3F antibodies block biofilm formation.**
530
531 A. To generate a strain which expresses KP T3F the structural genes *mrkABCDF* were inserted at the
532 3' *glmS* site in CR under the control of the T3SS effector protein Map promoter. This generated the
533 strain CR_{3F}.
534
535 B. *mrkA* transcripts were assessed by qRT-PCR from bacterial cultures of CR_{T3F} under T3SS
536 suppressing (LB) and inducing (DMEM) conditions. CR_{WT} is also shown as a negative control. T3SS

537 inducing conditions specifically induce *mrkA* transcription in CR_{T3F}. 4 biological replicates, central
538 tendency mean, error bars SEM. Paired T-test between LB and DMEM-grown CR_{T3F}.
539
540 C. mCherry expressing CR_{T3F} and CR_{WT} were grown in T3SS inducing conditions on glass coverslips
541 bottomed slides. Following 6 h attachment to glass was assessed and the adhered bacteria were
542 stained for MrkA. A dense lawn of CR_{T3F} is observed binding to the glass slide with MrkA detected on
543 the cell surface indicating functional surface KP T3F expression. The parental CR_{WT} strain adheres to
544 glass slides only sparsely.
545
546 D. At 8 dpi faecal CR_{T3F}+p*espO* levels are similar to CR_{WT} . Central tendency: median. n=15 mice per
547 group, 3 biological repeats. Mann-Whitney test, ns=non-significant. GoF, gram of faeces.
548
549 E. At 30 dpi blood was taken from mice that cleared infection with CR_{WT} or CR_{T3F}+p*espO*. An ELISA
550 was conducted against heat-killed KP_{WT} (expressing KP T3F) and an isogenic mutant lacking T3F
551 expression ($KP_{\Delta A-F}$). CR_{WT} infected mice had no detectable IgG responses to KP_{WT} or $KP_{\Delta mrkA-F}$. CR_{T3F}
552 +p*espO* infected mice had specific IgG responses against $KP_{WT.}$ n=15 mice per group, 3 biological
553 repeats. Central tendency: mean. Mann Whitney test.
554
555 F. Sera from CR_{WT} and CR_{T3F}+p*espO*-infected mice were used to stain KP_{WT} and image by
556 immunofluorescence microscopy. An α-MrkA pAb was used as a positive control. CR_{WT} derived sera
557 results in no detectable staining of KP_{WT} whereas sera from CR_{T3F}+p*espO*-infected mice and the α-
558 MrkA pAb phenocopy each other with spiculated membrane-associated staining of KP_{WT}.
559
560 G. CR preadsorbed sera from CR_{WT} and CR_{T3F}+p*espO*-infected mice were preincubated with KP_{WT} or
561 $KP_{\Delta mrkA-F}$ expressing sfGFP. A no-antibody control was used as an additional control. Following 6 h of
562 growth in M9 minimal media sfGFP signal was assessed on a plate reader and presented as the KP_{WT}
563 binding normalised to $KP_{\Delta mrkA-F}$ binding. The preadsorbed sera collected from CR_{T3F}+p*espO*-infected
564 mice specifically inhibited binding compared to $CR_{WT.}$ 4 biological replicates, central tendency: mean,
565 error bars: SEM. Repeated-measures One-way ANOVA corrected with Dunnett's multiple
566 comparisons test.
567
568 H. The biofilm formation from (G) was assessed by imaging using sfGFP fluorescence. A large
569 reduction in adhered KP_{WT} is observed when CR_{T3F} p*espO*-infected cross adsorbed sera was incubated
570 with KP_{WT} compared to CR_{WT} cross adsorbed sera.
571
572 ns=non-significant; *, p<0.5; ****, p<0.0001.
573
574 **Figure 7. The citrOgen platform as a versatile, quick and cost-efficient method of Ab production**
575 **and multiple downstream applications**
576
577 **A. citrOgen strain generation**. Selected Ag sequences are incorporated into the appropriate gene
578 editing vectors designed for optimal chromosomal expression of heterologous O-Ag, capsule
579 or complex protein Ags, the latter under the map promoter to ensure timely expression
580 during mucosal infection. p*espO* is then transformed to finalise the new citrOgen strain. QC
581 checks include assessment of heterologous expression and pedestal formation *in vitro* (as shown in
582 Supp Fig 1A, 4A and 5B) before proceeding to *in vivo* Ab production.

583 **B. In vivo Ab production.** The CR infection cycle and immune responses are co-opted by the citrOgen
584 platform: (i) EspO-mediated boosting of CR attachment to intestinal epithelial cells, (ii) continuous
585 exposure of immune cells to the heterologous Ags, (iii) B cell affinity maturation results in Abs,
586 primarily IgG, which mediate CR clearance by 28 dpi and can be obtained as pAb sera from blood.

587 **C. Downstream applications.**

588 Following citrOgen infection/immunisation, the functionality of Abs can be assessed *in vitro* or by *in*
589 *vivo* challenge studies, the pAb sera can be used for serotyping and the B cells can be used for mAb
590 production, either by using hybridoma technology to immortalise single-cell cloned B-cells or by
591 expressing heterologous Ag-specific Ab sequences in cell lines to obtain recombinant mAb.

592 Ab: Antibodies; mAb: monoclonal antibodies; pAb: polyclonal antibodies; Ag: Antigen; CR:
593 *Citrobacter rodentium*.

Materials and Methods

Bacterial culture and antibiotics

Bacteria were routinely cultured in LB Broth (Miller) (84649.05000, VWR, UK). Saturated (overnight, 18 hour) cultures took place by inoculating broth and incubation at 37°C and shaking at 200rpm.

Antibiotics were added to LB broth or LB broth solidified with agar (1.10283.0500, VWR, UK) at the following concentrations:

Gentamicin 10mcg/ml (cloning) (G1272, Merck, UK)
Streptomycin 50mcg/ml (cloning) (S6501, Merck, UK)
Kanamycin 50mcg/ml (cloning) Merck, UK)
Nalidixic acid 50mcg/ml (selecting CR and CFU enumeration from *in vivo* sample) (N4382, Merck, UK)
Rifampicin 50mcg/ml (selecting KP and CFU enumeration from *in vivo* sample) (R3501, Merck, UK)

Cloning

High-fidelity polymerase chain reaction was conducted using Phanta Flash (2x Phanta Flash Master Mix (Dye Plus), Vazyme, China). Screening and colony polymerase chain reaction was conducted using Rapid Taq (2x Rapid Taq Master Mix, Vazyme, China).

PCR purification (Monarch PCR & DNA Cleanup Kit (5ug), NEB) and plasmid extraction were conducted with kit-based methods.

All mutagenesis vectors were generated by PCR products ligation via Gibson Assembly (NEB, UK) according to the manufacturer's guidance.

Genome editing

The whole genome references sequences used for CR strain ICC168 (Nalidixic acid-sensitive version of ICC169) is FN543502. The whole genome reference sequence used for ICC8001 is the closely related ATCC43186-derivitive KPPR1 is CP009208.1. A list of strains generated in this work can be found in Supplementary Table 1.

Two methods of genome editing were conducted in this work. Insertions at the CR 3' *glmS* site were conducted using Tn7 mutagenesis with methods published in Choi et al. Nat Methods 2005 Jun;2(6):443-8[24]. Seamless, markerless genome editing at other sites was conducted by homologous recombination based on the pSEVA612S system (https://seva-plasmids.com/) in both CR and KP as previously published in detail[12,25]. To improve the efficiency of pSEVA612S for Gibson Assembly we further modified this plasmid by reversing the sequence of the 3' ISceI endonuclease digestion site generating pSEVA612S(R). This modification improves efficiency by reducing homology-based empty vector recombination.

All mutagenesis vectors are summarised in Supplementary Table 2 and are publicly available at https://doi.org/10.6084/m9.figshare.c.7869659.v1. In the case where more than one vector was used these are listed against the respective strain. To generate CR_{KPK2} we initially cloned a construct (pSEVA612S(R)_CRColanic::K2cpsΔwbbJ_ORF) without the genes wbbJ and an annotated open reading frame of unknown function[41]. We subsequently inserted these genes into our final CR_{KPK2} strain (pSEVA612S(R)_ΔwbbJ::Ins_wbbJ_ORF) as new data become available[42] and included the native KP promoter (pSEVA612S(R)_K2:col_Pvariant_Porf2).

644
645 Transformation of pACYC184_espO was conducted using room temperature competent cells
646 according to our previously published protocol[25].
647
648 All primers are appended to GenBank files and publicly available at
649 https://doi.org/10.6084/m9.figshare.c.7869659.v1.
650
651 **Sequencing**
652
653 Sanger sequencing of PCR products and plasmids was conducted by Eurofins Genomics.
654
655 **In silico serotyping**
656
657 In silico serotyping of CR was conducted using SerotypeFinder 2.0
658 (https://cge.food.dtu.dk/services/SerotypeFinder/) on genome FN543502.
659
660 **Crude LPS preparation and Silver stain**
661
662 1 ml of overnight bacterial cultures normalised to OD_{600} of 1.2 were pelleted by centrifugation at
663 10,000 g and resuspended in 200 µl Laemmli buffer, followed by boiling at 100°C for 5 minutes.
664 Proteinase K was added to a final concentration of 1 mg/ml, and samples were incubated at 60°C for
665 2 hours. Subsequently, 5% β-mercaptoethanol was added, and samples were incubated for an
666 additional 5 minutes. Crude LPS samples were separated by SDS- polyacrylamide gel electrophoresis
667 (PAGE) using a 12% gel, and the resulting gels were fixed in 5% acetic acid/40% isopropanol
668 overnight. Silver staining was then performed using the SilverQuest™ Silver Staining Kit (LC6070,
669 Thermo Fisher Scientific) according to the manufacturer's protocol. All steps were carried out at
670 room temperature with gentle agitation. Images were acquired on a ChemiDoc XRS+ and visualised
671 using Image Lab software (Bio-Rad Laboratories).
672
673 **LPS extraction and Western Blotting**
674
675 LPS was extracted from 3OD units of saturated overnight cultures using a modified phenol method
676 kit (iNtRON Biotechnology, Korea) according to the manufacturer's guidance with no modification.
677
678 Samples were mixed with 5x Laemmli buffer and 5% 2-mercaptoethanol and separated by SDS–PAGE
679 using a 12% acrylamide gel and tris-glycine buffer system. and transferred to polyvinylidene
680 difluoride membranes (#1620177, Bio-Rad Laboratories) using a TransBlot semi-dry electrophoretic
681 transfer machine (Bio-Rad). Membranes were blocked for 2 h at room temperature (RT) in 10% fat-
682 free milk PBS–0.1% Tween 20 (PBS-T) and incubated overnight at 4°C with 1:500 anti-O152 or 1:2000
683 anti-KP O1 (Supplementary Table 3) in PBS-T with 5% BSA (A3059-50G, Sigma). Secondary antibodies
684 (Supplementary Table 3) were added diluted 1:10000 in 5% fat-free milk in PBST and incubated for 1
685 h at RT. Immunoblots were developed with Clarity Western enhanced chemiluminescence (ECL, Bio-
686 Rad Laboratories) and images were acquired on a ChemiDoc XRS+ and visualised using Image Lab
687 software (Bio-Rad Laboratories).
688
689 **In vitro CR_{KPO1}, $CR_{KP\ K2}$ and CR_{T3F} infections of fibroblasts**
690
691 Murine Swiss 3T3 fibroblasts (ATCC® CCL-92™) were maintained in DMEM containing 4500 mg l^{-1}
692 glucose (D6546, Sigma) and supplemented with 10% fetal calf serum (F9665, Sigma) and 2 mM
693 glutaMAX (#35050061, ThermoFisher Scientific) at 37°C in 5% (v/v) CO_2 and seeded on glass
694 coverslips in 24-well plates (density $2x10^5$cells/well) for immunofluorescence. Indicated strains of CR

695 expressing mCherry from a pUltra plasmid[43] were grown to saturation in LB supplemented with
696 gentamicin at 37°C with 200 rpm agitation for 8 hours before subculturing 1:500 for 16 hours in LB or
697 DMEM with 1000 mg l^{-1} glucose (# D5546, Sigma) at 37°C, 5% (v/v) CO_2, static. Cells were infected
698 with the static culture at a multiplicity of infection (MOI) of 100, confirmed by retrospective plating.
699 The plate was centrifuged at 1000 rpm for 5 min at RT to synchronize infection and incubated for 4
700 hours at 37°C in a 5% CO_2 atmosphere. The infection was stopped with three washes with sterile
701 phosphate-buffered saline (PBS) and cells were fixed in PBS with 4% (w/v) paraformaldehyde for 15
702 mins at RT and washed three times in PBS. Cells were then permeabilized in 0.1% (v/v) of Triton X100
703 in PBS for 10 min, incubated in 50 mM NH_4Cl in PBS as a quenching agent for 10 min, washed in PBS,
704 and blocked in 3% BSA in PBS for 1 h at RT before staining with one of the following primary
705 antibodies in 1% BSA-PBS for 1 h at RT: anti-KPO1 C13 (1:200), anti-mrkA (1:100) or anti-KP K2
706 (1:100) (Supplementary Table 3). Coverslips were washed in PBS and incubated with Alexafluor488-
707 conjugated secondary antibodies (1:200), Tetramethylrhodamine (TRITC)–conjugated phalloidin
708 (1:500) and 4,6-diamidino-2-phenylindole (DAPI) (1:1000) to label the heterologously-expressed
709 antigen, F-actin and DNA, respectively (Supplementary Table 3) in 1% BSA-PBS for 1 h. Coverslips
710 were washed in PBS and once in water before being mounted using Gold Pro-Long Anti-fade medium
711 (#P36930, ThermoFisher Scientific) and left to cure overnight at RT in the dark. Immunofluorescence
712 images were acquired using a Zeiss AxioImager Z1 microscope and processed using ZEN3.1 software
713 (ZEN lite, Zeiss).
714
715 **Reverse transcription quantitative PCR (RT-qPCR)**
716
717 The indicated strains of CR were grown to saturation overnight in LB supplemented with the
718 corresponding antibiotics. 0.5 ml of the overnight culture were washed once in PBS, incubated in
719 RNAprotect Bacteria reagent (#76506, Qiagen) for 10 mins at RT and centrifuged at 3000 xg for 5
720 min. The bacterial pellet was digested in 100 µl TE buffer ((30 mM Tris·Cl, 1 mM EDTA, pH 8.0) with
721 15 mg/ml Lysozyme (L6876, Sigma-Aldrich) and 20 µl Proteinase K (#19131, Qiagen) for 10 min
722 according to manufacturer's guidelines. RNA was isolated using the RNeasy minikit (Qiagen)
723 following the manufacturer's instructions, and RNA concentration and purity was determined using a
724 Nanodrop 2000 spectrophotometer (ThermoFisher Scientific). 1 µg of RNA was treated with RNase-
725 free DNase (#M6101) for 1 h at 37 °C and cDNA was then synthesized using a Moloney murine
726 leukemia virus (M- reverse transcriptase (M-MLV, #M1705) with random primers (#C1181) following
727 the manufacturer´s instructions (all from Promega). To confirm the absence of undigested DNA, a
728 reaction mixture without the M-MLV reverse transcriptase was also included (NRT). qPCR was
729 performed using the Power Up SYBR Green master mix (#A25778, ThermoFisher Scientific) and the
730 relevant primers, whose primer efficiency had been evaluated previously and determined to be 95-
731 105% (Supplementary Table 4). The assay was run on a Quantstudio 1 System (Applied Biosystems,
732 ThermoFisher Scientific) and results were analysed using the QuantStudio Design & Analysis
733 Software v1.5.2 (Applied Biosystems, ThermoFisher Scientific). The relative expression level of each
734 mRNA was evaluated using the 2-ΔCtmethod, where Ct is the threshold cycle and 16S rRNA is used
735 as the control.
736
737 **O25 antisera agglutination**
738
739 Heat-killed agglutination was performed on the indicated strains after overnight growth in LB. The
740 anti-O25 sera (85022, SSI Diagnostica) was used according to the manufacturer's protocol. Images
741 were acquired on a ChemiDoc XRS+ and visualised using Image Lab software (Bio-Rad Laboratories).
742
743
744 **Whole bacterial cell ELISA**

To prepare heat-killed KP the indicated strains were grown overnight in LB at 37°C at 200 rpm. The culture was then normalised to an optical density of 1 at 600 nm in sterile PBS, heat inactivated in the presence of EDTA-free protease inhibitor cocktail (#4693159001, Sigma) at 60°C for 1 h and stored at 4°C until use (short-term). ELISA Flat-Bottom Maxisorp Immuno 96- Well Plates (#10547781, Fisher Scientific) were incubated with 100 µL/well heat-killed CR for our serum samples or with 100 µL/well goat anti-mouse IgG antibody for the standards (2 µg/µL) (Supplementary Table 3) overnight at 4°C. Plates were washed three times with PBS-T, blocked for 1 h at RT with 5% BSA-PBS-T, and incubated overnight at 4°C with serum samples or serially diluted mouse IgG (Supplementary Table 3) as standard. Plates were washed as described above and incubated with horseradish peroxidase (HRP)-conjugated goat anti-mouse IgG antibody (Supplementary Table 3) for 1 h at room temperature. Plates were washed and developed by the addition of 100 µL 3,3 ,5,5 -tetramethylbenzidine (TMB; Thermo Fisher Scientific) for 5-15 mins before stopping the reaction with 2 N H_3PO_4. The absorbances at 450 and 540 nm were measured in a plate reader (FLUOstar Omega; BMG Labtech), and anti-KP IgG levels were quantified in samples by comparison to a mouse IgG standard curve.

Determination of O-antigen-binding specificity: KP_{WT} expressing mCherry and $KP_{\Delta rfb}$ expressing sfGFP were grown as saturated overnight cultures in LB supplemented with gentamicin. On the following day, both strains were mixed 1:1 (v/v) after confirming the had grown to the same optical density (600nm) and transferred to a V-bottom 96-well plate (Greiner Bio-one) for staining. Single strain controls were also included to ensure correct gating during flow cytometry analysis. Samples were first blocked in 5% BSA/PBS for 1 h at RT shaking, centrifuged at 4000 rpm, 4 °C, 10 mins and then incubated overnight with sera from CR_{WT} or CR_{KPO1}+pespO-infected mice diluted 1in100 (v/v) in 1% BSA/PBS. Bacterial samples were centrifuged, washed twice in cold PBS and resuspended in 1% BSA/PBS containing AlexaFluor647-conjugated anti-mouse IgG (1:200, Supplementary Table 3) for 1 h at RT shaking. Cells were washed twice in cold PBS, fixed in 1% PFA/PBS and kept in the dark until flow cytometry analysis. Samples were acquired (minimum of 100000 bacterial cells per sample) on a Cytek Amnis CellStream and data was analysed using FlowJo v10.10.0 (gating strategy shown in Supplementary Fig 3A).

K2 serotyping: The KP MRSN Diversity Panel (NR-55604) was obtained through BEI Resources, NIAID, NIH[33]. The 100 strains from the MRSN collection, KP_{WT} and $KP_{\Delta wcaJ}$ (positive and negative controls respectively) were grown overnight in 1mL of LB in deep well 96-well plates (VWR). 100ul of each overnight was transferred to a V-bottom plate and used for staining. Plates were centrifuged at 4000 rpm for 10 mins at 4°C, resuspended in 5% BSA/PBS and blocked for 1 h at RT shaking using a microplate mixer. Bacterial samples were then centrifuged and stained overnight at 4°C shaking using sera from CR_{KPK2}+pespO-infected mice diluted 1in100 (v/v) in 1% BSA/PBS. On the following day, bacterial samples were washed two times in cold PBS and stained for 1 h at RT shaking with AlexaFluor-488-conjugated anti-mouse IgG (1:300; Supplementary Table 3). Cells were washed twice in cold PBS, fixed in 1% PFA/PBS and kept in the dark until flow cytometry analysis. Samples were acquired on a Cytek Amnis CellStream (minimum of 50000 bacterial cells per sample) and data was analysed using FlowJo v10.10.0.

Bacterial cell immunofluorescence microscopy (adherent protocol and suspension protocol)

We used two protocols for immunofluorescent staining of KP.

Adherent protocol (all ICC8001 staining)

mCherry expressing ICC8001 was grown as a saturated overnight culture which was sub-cultured (1;1000 v/v) into M9 media (M9 salts M6030, Sigma, UK) supplemented with 0.4% glucose w/v

796 (G8270, Sigma, UK). 400ul was added into each well for imaging in a coverslip slide (µ-Slide 8 Well
797 high Glass Bottom, ibidi). Slides were grown statically at 37°C for 4 hours and cells were washed in
798 phosphate-buffered saline before staining. Primary staining (sera, antibodies) took place overnight at
799 4°C in 0.22um filtered 3% bovine serum albumin (A3059, Sigma, UK)/ PBS on a rocking platform.
800 Primary antibody was removed and slides were washed 3x in PBS followed by incubation with
801 fluorescently labelled secondary antibodies (Supplementary Table 3) in 3%BSA/PBS at room
802 temperature for 1 hour on a rocking platform. Slides were washed 3 times before imaging.
803
804 **Suspension protocol (MRSN collection, Figure 4D)**
805
806 MRSN collection strains were grown as saturated overnight cultures. 100ul of overnight was used for
807 staining. Following centrifugation (5000g, 5 minutes) cells were washed 3 times in PBS. Primary
808 staining (K2 antisera) took place overnight at 4°C in 3%BSA/PBS in 400ul volume with agitation. Cells
809 were washed by sequential spins (5000g, 5 minutes) and resuspension in PBS (3 washes). Secondary
810 antibody (Supplementary Table 3) was added for 45mins at room temperature in a 100ul volume
811 with agitation. Cells were washed by sequential spins (5000g, 5 minutes) and resuspension in PBS (3
812 washes). Cell membranes were then labelled with FM® 4-64 Dye (T13320, ThermoFisher Scinentific,
813 UK) at a final concentration of 5ug/ml in 100ul of PBS for 10 mins at room temperature in the dark.
814 Cells were washed once and resuspended in 100ul of fresh PBS before imaging. Cell suspension was
815 imaged on an 1% agarose (in dH_2O) pad according to the following protocol
816 (https://biotium.com/tech-tips/tech-tip-imaging-bacteria-using-agarose-pads/).
817
818 **CR_{T3F}+p*espO* glass binding assay**
819
820 mCherry expressing CR_{T3F}+p*espO* and CR_{WT} were grown as saturated overnight cultures and sub-
821 cultured (1:100) into DMEM low glucose (D5546, Merck, UK) into glass coverslip slides (µ-Slide 8 Well
822 high Glass Bottom, ibidi). Slides were grown statically at 37°C for 6 hours and cells were washed in
823 phosphate-buffered saline before fixing in 4% paraformaldehyde/PBS (R1026, Agar Scientific, UK) for
824 20 mins at room temperature. Cells were stained for MrkA according to the adherent protocol
825 outlined above.
826
827 **Pre-adsorption of CR sera**
828
829 Serum samples from mice infected with CR_{T3F}+pespO with anti-KP antibodies above 200ng/mL were
830 pooled; sera from CR_{WT}-infected mice were also pooled separately as a control. To inactivate
831 complement, pooled serum samples were heated at 55°C for 1 h and then were pre-adsorbed onto
832 CR_{WT} expressing sfGFP to remove CR-specific antibodies, thus enriching for anti-KP antibodies. This
833 was done by serially incubating the pooled sera samples, both from CR_{WT}- and CR_{T3F}+pespO-infected
834 mice, with ~$5x10^8$ CR_{WT} for 24 h at 4°C on a rotating wheel for 10 rounds of pre-adsorption. After
835 each 24h-incubation, the serum samples with CRWT were centrifuged at 3000 xg for 5 mins to pellet
836 the bacteria, which were kept at 4°C until flow cytometry analysis; the supernatant containing the
837 antibodies was subsequently incubated with a fresh batch of ~$5x10^8$ CR_{WT} expressing sfGFP. At the
838 end of the 8 rounds, sfGFP-expressing bacterial samples from each round of pre-adsorption with sera
839 from CR_{WT}- and CR_{T3F}+*pespO*-infected mice were stained with AF555-conjugated anti-mouse IgG
840 (1:400; Supplementary Table 3) in 2% BSA-PBS for 30 mins and analysed using a Cytek Amnis
841 CellStream. Obtained data was subsequently analysed using FlowJo v10.10.0.
842
843 **Dot blot**

844 Bacterial cultures were grown overnight in LB (CR) or M9 supplemented with glucose (KP),
845 normalised to an OD600 of 1 and centrifuged to pellet the cells. The pellet was resuspended in 1 ml
846 PBS and equal volumes of bacteria were then spotted onto a nitrocellulose membrane (#88018,
847 ThermoFisher Scientific) and allowed to air dry. The membrane was blocked at RT for 2 h in 5% milk-
848 PBS-T and incubated overnight at 4°C with the indicated sera diluted in 5% BSA-PBS-T to a
849 concentration of 2µg/ml of total IgG. The primary was washed three times in PBS-T and a secondary
850 HRP-conjugated anti-mouse antibody (Supplementary Table 3) was added in 5% milk-PBS-T,
851 incubated for one hour at RT, and washed three times. Detection was carried out using ECL substrate
852 (Bio-Rad) and images were acquired on a ChemiDoc XRS+ and visualised using Image Lab software
853 (Bio-Rad Laboratories).
854
855 **Fluorescent biofilm formation assay**
856
857 KP_{WT} and $KP_{\Delta mrkA\text{-}F}$ expressing sfGFP were grown overnight in M9 media and diluted into fresh M9
858 1:500 (v/v) and preincubated for 30 mins with no sera or with ~50 µg/mL IgG (1:100 dilution) of the
859 pre-adsorbed sera from either CR_{WT}- and CR_{T3F}+p*espO*-preinfected mice at RT on a rotating wheel.
860 100 µl of each sample in triplicate were transferred into wells in a black/clear-bottom 96-well tissue-
861 culture treated plate (#353219, SLS) and incubated statically at 37℃ for 6 h. Samples were then
862 washed 5 times with sterile PBS and bottom optic fluorescence readings were taken at 485/520
863 (Ex/Em) using a FLUOstar Omega plate reader. Fluorescence values were normalised to those
864 obtained with the $KP_{\Delta mrkA\text{-}F}$ strain, which does not attach, to remove any non-specific fluorescence
865 and reduce batch-to-batch variation.

866 **Animal work**
867
868 All animal work took place at Imperial College London (Association for Assessment and Accreditation
869 of Laboratory Animal Care accredited unit) under the auspices of the Animals (Scientific Procedures)
870 Act (UK) 1986 (PP7392693). Work was approved locally by the institutional ethics committee.
871
872 **Animals**
873
874 Female CD-1 and C57BL/6 mice were purchased from Charles River, UK. Mice were purchased at 29-
875 31 g weight (5-7 weeks) (CD-1 mice) and 18-20 g weight (6-8 weeks) (C57BL/6 mice). For each
876 experiment, mice were randomly assigned to experimental groups. Investigators were not blind to
877 the allocation. C57BL/6 were used for the data shown in Supplementary Figure 2C, all experiments
878 directly related to the citrOgen platform were performed in CD-1.
879
880 **Husbandry**
881
882 Animal technicians within the facility received mice and blindly separated them into groups of 5 into
883 high-efficiency particulate air (HEPA)–filtered cages with sterile bedding. Bedding was changed
884 weekly, and enrichment supplied. Mice were housed under a 12/12-hour light/dark cycle with
885 access to food and water *ad libitum*. Researchers (JSG and JLCW) conducting the work in this study
886 were not involved in selection of animals into groups as this was undertaken by technical staff prior
887 to starting experiments. Animals were identified by ear notching (conducted under restraint with no
888 anaesthesia).
889
890 **CR infection by oral gavage**
891
892 For infections, the indicated CR strains were grown overnight in 15 ml of LB (50 ml capped Falcon
893 tubes) at 37°C and 200 rpm. The next day, the tubes were centrifuged, and the pellet was
894 resuspended in 1.5 ml of sterile PBS. Mice were infected by oral gavage with 200 µl of this solution
895 ($1x10^9$ CFU confirmed by viable counts as previously described[13]). CR faecal shedding was
896 determined by collecting stool samples at the specified days post-infection (DPI), homogenising the
897 samples in PBS and plating serial dilutions onto LB agar containing nalidixic acid. Plates were
898 incubated at 37°C overnight and colonies were counted on the following day.
899
900 Mice were culled at 6 (C57BL/6) or 8 dpi (CD-1) and colons were extracted for downstream
901 processing. When characterising antibody responses, mice were followed until clearance of CR
902 infection and then culled to obtain sera or challenged with KP infection.
903
904 **Colonic histology processing and immunostaining**
905
906 At 8 DPI, the colon was extracted, and the distal 0.5 cm was fixed in 4% PFA for 2 hours and then kept
907 in 70% ethanol until processing. Fixed tissues were processed, paraffin embedded and sectioned at 5
908 µm. For immunofluorescence, sections were dewaxed by submersion in HistoClear II solution
909 (#101412-884, VWR) twice for 10 min, 100% ethanol twice for 10 min, 95% ethanol twice for 10 min,
910 80% ethanol once for 3 min, and PBS-0.1% Tween 20-0.1% saponin (PBS-TS) twice for 3 min.
911 Subsequently, sections were heated for 30 min in demasking solution (0.3% trisodium citrate-0.05%
912 Tween 20 in distilled H2O). Once cooled, slides were first blocked in PBS-TS supplemented with 10%
913 normal donkey serum (NDS, D9663, Sigma) for a minimum of 1 h in a humid chamber, before being
914 incubated with anti-CR antibody (1:50) and anti-KP O1 (1:100) diluted in PBS-TS with 10% NDS
915 overnight at 4°C. Slides were rinsed twice for 10 min each time in PBS-TS, followed by incubation
916 with Alexafluor488-conjugated secondary antibodies (1:100) and DAPI (1:1000) (Supplementary

917 Table 3). Washing steps were repeated before slides were mounted with ProLong Gold antifade
918 mountant. Images were acquired using a Zeiss AxioVision Z1 microscope using a Hamamatsu
919 microscope camera and processed using ZEN3.1 software (ZEN lite, Carl Zeiss MicroImaging GmbH,
920 Germany).
921
922 **cIEC isolation and flow cytometry analysis**
923
924 Colonic intestinal epithelial cells (cIECs) from mock-infected and CR-infected C57BL/6 mice were
925 isolated from 2-cm distal colonic tissue samples as previously described[44]. Briefly, the 2-cm colonic
926 tissue sample was opened longitudinally and washed in 1× Hanks' balanced salt solution (HBSS)
927 without Mg and Ca (# 14185045, ThermoFisher Scientific) and incubated at 37°C, 200 rpm for
928 45 min in IEC dissociation buffer (1× HBSS, 10 mM HEPES, 1 mM EDTA, and 5 µL/mL 2-β-
929 mercaptoethanol). The remaining tissue was removed, and detached cells were collected by
930 centrifugation (3000 rpm for 10 min), followed by two DPBS (#D8537, Sigma) washes at 4°C. Cells
931 were then incubated 5 mins at RT with 50 µg/mL DNase I (#11284932001, Sigma) to digest
932 extracellular DNA and passed through a 70-µm cell strainer on ice to ensure a single-cell suspension,
933 pooling samples from the same group and rinsing with 20 mL of cold DPBS. All steps from here
934 onwards were performed on ice/at 4°C to maintain cell viability. cIECs were counted using trypan
935 blue to exclude dead cells and ~$1x10^7$ live cells were centrifuged, resuspended in fluorescence-
936 activated cell sorter (FACS) buffer (5% FBS, 2mM EDTA in DPBS) supplemented with Fc block (#130-
937 092-575, Miltenyi Biotec) and incubated for 10 min. Samples were then incubated with FACS buffer
938 containing anti-CR (1:1000) for 20 mins, washed twice in and then incubated with EpCAM-APC
939 (1:100) and phycoerythrin (PE) anti-rabbit IgG (Supplementary Table 3) for 40 min, washed, and
940 fixed in 1% paraformaldehyde in PBS prior to analysis on a BD LSRFortessa cell analyser (BD
941 Biosciences). Data were analysed using FlowJo v10.10.0 and the gating strategy is shown in
942 Supplementary Fig. 2A.
943
944 **Tail vein bleeds and serum separation**
945
946 Small volume bleeds (<100ul) were conducted on conscious, restrained mice using a Tail Vein
947 Injection platform (Hugeiron, MouseSerum, China). Blood was taken from the lateral tail vein by
948 puncture with a 25G needle and collected via pipette into a paediatric serum collection tube
949 (Microvette® 100 Serum Cat, Starstedt). Following 1 hour of clotting at RT, sera was separated by
950 centrifugation at 20 000g for 3 minute. Separated sera was stored at -80°C until use.
951
952 **KP pulmonary infections**
953
954 Anaesthesia (ketamine 80mg/kg and medetomidine 0.8mg/kg) was delivered by intraperitoneal
955 injection. Body temperature was maintained with a heat mat throughout until recovery or during the
956 intubation procedure itself.
957
958 Intubation was achieved with a 20G cannula (BD Insyte, BD) using the commercially supplied
959 intubation kit (Endotracheal Mouse Intubation Kit, ETI-MSE, Kent Scientific). 50ul of inoculum
960 (diluted in phosphate buffered saline) was delivered into the hub of the 20G cannula and drawn into
961 the lungs by spontaneous ventilation.
962
963 Recovery took place at 32°C in a forced air heating cabinet. At 15 minutes post anaesthesia induction
964 medetomidine was reversed by the administration of 0.8mg/kg atipamezole, delivered by
965 subcutaneous injection into the neck scruff.
966

967 The total volume of administered drugs was designed to deliver 20mg/kg of total fluids to animals, a
968 human paediatric resuscitation dose.
969
970 Mice were returned to their home individual ventilated cages after they were spontaneously moving
971 and checked at regular intervals post infection.
972
973 **Cardiac puncture**
974
975 Mice were weighed at end-point (after clearance for CR infected animals and 72 hpi for KP-
976 challenged animals).
977
978 Anaesthesia (ketamine 100mg/kg and medetomidine 1mg/kg) was delivered by intraperitoneal
979 injection. Mice were checked and following the absence of pedal reflexes placed in dorsal
980 recumbency. Paws were taped to a board and scissors used to remove the skin over the
981 xiphisternum. Blood was collected from the right ventricle (closed approach) with a 25G needle
982 inserted at 30° to the skin surface until blood was freely aspirated into a 1ml syringe.
983
984 When blood was obtained for determination of IgG titres (i.e mice infected with indicated CR strains
985 expressing heterologous antigens), the 25G needle was removed (to prevent haemolysis) and the
986 blood was transferred to a serum collection tube containing a clot activator (BD Microtainer SST with
987 separating gel, BD). Blood in the serum tube was allowed to clot for 1 hour at RT before
988 centrifugation (20 000 xg) for 3 minutes. The sera was divided into aliquots and stored at -80°C until
989 use.
990
991 When blood was obtained from KP challenged mice, 20ul of whole blood was taken for CFU
992 enumeration by plating 10-fold serial dilutions (in PBS supplemented with 1mmol EDTA to prevent
993 clotting) on LB Agar plates containing rifampicin 50ug/ml. The 25G needle was again removed and
994 approximately 50-100 µl placed immediately into a tube coated with EDTA for anticoagulation
995 (Microvette® 100 EDTAK3E, 100ul, Sarstedt) for haematological analysis. The remaining blood
996 (approximately 800 µl) was allowed to clot for 1 hour at room temperature in a serum collection tube
997 as described above, before centrifugation (20 000g) for 3 minutes. The sera was divided into aliquots
998 and stored at -80°C until use.
999
1000 **Lung homogenate processing**
1001
1002 Post-mortem lungs were removed and placed in 3ml of phosphate buffered saline in a gentleMACS
1003 C-tube (Miltenyi Biotec). These were homogenised on a gentleMACS Octo Dissociator (Miltenyi
1004 Biotec) using the program m_lung_2. The program was run twice in succession to achieve uniform
1005 homogenisation.
1006
1007 30ul of lung homogenate was taken for CFU enumeration by plating 10-fold serial dilutions on LB
1008 Agar plates containing rifampicin 50ug/ml.
1009
1010 1ml of lung homogenate was transferred into a 1.5ml microcentrifuge tube and spun at 10 000 xg for
1011 5 minute at 4°C to pellet out particulate matter. The supernatant was stored -80°C for future use.
1012
1013 **HM5 analysis of EDTA anticoagulated whole blood**
1014
1015 Anticoagulated blood was run on the HM5 Vetscan analyser according to the manufacturer's
1016 instruction.

1017 Outcome variables of infection were assessed using the kits summarised in Supp Table 5 according to
1018 the manufacturer's guidelines with the following specifications.
1019
1020 **Capture ELISAs:** ELISAs were performed using ELISA Clear Flat-Bottom Maxisorp Immuno 96- Well
1021 Plates (#10547781, Fisher Scientific). Samples were added to coated and blocked plates and
1022 incubated overnight at 4 degrees for all ELISAs. The range of sample dilutions used for each ELISA is
1023 indicated in Supplementary Table 5; serial dilutions in the corresponding assay diluent were
1024 performed when samples needed to be diluted further than 1in50. After addition of the TMB
1025 substrate solution (#00-4201-56, ThermoFisher Scientific) to the wells at the end of the assay, these
1026 were incubated at RT until a clear gradation in colour could be seen from the highest to the lowest
1027 standard, at which point the reaction was stopped by adding 1M phosphoric acid (Sigma). All
1028 absorbance readings were obtained using a using a FLUOstar Omega plate reader and readings at
1029 540 nm were subtracted from absorbance readings at 450nm to correct for optical imperfections of
1030 the plate. All ELISAs included blanks and standard curves with at least 7 points within range. Sample
1031 values were obtained by interpolation into the standard curve; any samples with values out of the
1032 range of the standard were assayed again at a dilution(s) that ensured the value was within range.
1033
1034 **Albumin:** All reactions were done in a total volume of 200 µl in an untreated 96 well plate (Greiner
1035 Bio-one) to allow vigorous shaking after reagent addition. Samples and standard were diluted 1:5 in
1036 PBS (0.01 M, pH 7.4) and 5 µl were added per well; 5 µl of double-distilled water were added to the
1037 blank. Subsequently 195 µl of stock working solution (prepared according to the manufacturer's
1038 instructions) were added into each well, mixed thoroughly using a plate mixer and then left to stand
1039 at RT for 10 mins before measuring the absorbance of each well at 628 nm using a FLUOstar Omega
1040 plate reader.
1041
1042 **Creatinine:** Serum samples did not require deproteinization. The assay was performed using the
1043 colorimetric reaction mix, and readings were acquired by measuring absorbance at 570 nm using a
1044 FLUOstar Omega plate reader. High levels of haemolysis lead to high background due to the colour;
1045 background control samples (ie sample with no creatininase) were essential in those cases. 40 µl of
1046 serum sample and 10 µl of assay buffer were used per sample well; standards were prepared
1047 according to the manufacturer's instructions. After interpolating into the standard curve and
1048 correcting for sample dilution, the values are given as nmol/ 50 µl sample; these were transformed
1049 to mg/dL, where the molecular weight of creatinine is 113.12 mg/mmol.
1050
1051 **Data analysis and visualisation**
1052
1053 Graphs and statistical analysis was carried out in GraphPad Prism version 10.4.1 for Windows and
1054 version 10.4.0 for Mac (GraphPad Software, Boston, Massachusetts USA, www.graphpad.com). Data
1055 were analysed for normal distribution based on D'Agostino-Pearson or Shapiro-Wilk normality tests
1056 before performing any statistical analyses. Normally distributed data was analysed with the
1057 parametric tests detailed in the figure legends; indicated non-parametric tests were applied to data
1058 that failed to meet the normality criteria. When more than three comparisons were made, *p* values
1059 were adjusted for multiple comparisons as indicated in the figure legends (Dunnett's post hoc test).
1060 For ELISAs, two or three technical replicates were used to estimate experimental mean. Statistical
1061 significance was only determined in datasets where each group had three or more biologically
1062 independent repeats. A p value <0.05 is considered statistically significant. Each parameter was
1063 measured only once in each distinct sample, but more than one parameter could be measured in the
1064 same sample (data in Fig.3). value <0.05 is considered statistically significant.

1065 Schematics in Supplementary Fig. 5C and Fig. 6 were made using some images from BioRender

1066 (created with BioRender.com). Images were edited and compiled into figures in Affinity Designer V2.

1067 (Serif Europe Ltd).

1068 **Data availability**

1069 All plasmid vector sequences are publicly available at
1070 https://doi.org/10.6084/m9.figshare.c.7869659.v1. The data that support this study are available in
1071 the supplementary Figures and Tables and from the corresponding authors upon request.

1072 **Acknowledgements**

1073 We would like to thank Professor Richard Strugnell and Dr Jonathan Wilksch at the University of
1074 Melbourne for providing the reference K2 antisera and C13 monoclonal antibody for use in this work.
1075 We would like to thank Professor Matthew Upton and Dr Katie Muddiman at the University of
1076 Plymouth for the EC958 isolate.

1077 We would like to thank our colleagues Dr Abigail Clements, Dr Andrew Conway Morris, Professor
1078 Victor de Lorenzo, Professor Gordon Dougan and Professor Jose Penadés for their critical assessment
1079 and feedback in writing this manuscript.

1080 We would like to thank our colleagues Dr Mei Chong and Mr Edmond Yau in the Imperial College
1081 London Enterprise team for their support in the patent application covering the technology
1082 described in this manuscript.

1083 **Conflicts of interest**

1084 The authors declare no competing interests.

1085 **Patent**

1086 The technology underlying citrOgen has a patent pending.

1087 **Funding**

1088 This project has been supported by grants from The Royal Society (IC160080) and Medical Research
1089 Council (MR/R02671)

1090 References

1091

1092 1. El-Atawi, K. *et al.* Efficacy and Safety of Palivizumab as a Prophylaxis for Respiratory
1093 Syncytial Virus (RSV) Disease: An Updated Systemic Review and Meta-Analysis. *Cureus*
1094 **15**, e51375 (2023).
1095 2. Thandavaram, A. *et al.* The Efficacy of Bezlotoxumab in the Prevention of Recurrent
1096 Clostridium difficile: A Systematic Review. *Cureus* **14**, e27979 (2022).
1097 3. Self, W. H. *et al.* Neutralizing COVID-19 Convalescent Plasma in Adults Hospitalized
1098 With COVID-19: A Blinded, Randomized, Placebo-Controlled Trial. *Chest* **162**, 982–994
1099 (2022).
1100 4. Focosi, D., Franchini, M., Casadevall, A. & Maggi, F. An update on the anti-spike
1101 monoclonal antibody pipeline for SARS-CoV-2. *Clin Microbiol Infect* **30**, 999–1006
1102 (2024).
1103 5. van der Horst, H. J. & Mutis, T. Enhancing <scp>Fc</scp> -mediated effector functions
1104 of monoclonal antibodies: The example of <scp>HexaBodies</scp>. *Immunol Rev* **328**,
1105 456–465 (2024).
1106 6. Stone, C. A., Spiller, B. W. & Smith, S. A. Engineering therapeutic monoclonal
1107 antibodies. *Journal of Allergy and Clinical Immunology* **153**, 539–548 (2024).
1108 7. Henry, C. *et al.* Influenza Virus Vaccination Elicits Poorly Adapted B Cell Responses in
1109 Elderly Individuals. *Cell Host Microbe* **25**, 357-366.e6 (2019).
1110 8. Tkaczyk, C. *et al.* Identification of anti-alpha toxin monoclonal antibodies that reduce
1111 the severity of Staphylococcus aureus dermonecrosis and exhibit a correlation
1112 between affinity and potency. *Clin Vaccine Immunol* **19**, 377–85 (2012).
1113 9. Zhu, H., Rollier, C. S. & Pollard, A. J. Recent advances in lipopolysaccharide-based
1114 glycoconjugate vaccines. *Expert Rev Vaccines* **20**, 1515–1538 (2021).
1115 10. Mundy, R., MacDonald, T. T., Dougan, G., Frankel, G. & Wiles, S. Citrobacter rodentium
1116 of mice and man. *Cell Microbiol* **7**, 1697–706 (2005).
1117 11. Sanchez-Garrido, J., Ruano-Gallego, D., Choudhary, J. S. & Frankel, G. The type III
1118 secretion system effector network hypothesis. *Trends Microbiol* **30**, 524–533 (2022).
1119 12. Ruano-Gallego, D. *et al.* Type III secretion system effectors form robust and flexible
1120 intracellular virulence networks. *Science* **371**, (2021).
1121 13. Crepin, V. F., Collins, J. W., Habibzay, M. & Frankel, G. Citrobacter rodentium mouse
1122 model of bacterial infection. *Nat Protoc* **11**, 1851–76 (2016).
1123 14. Dennis, A. *et al.* The p50 subunit of NF-kappaB is critical for in vivo clearance of the
1124 noninvasive enteric pathogen Citrobacter rodentium. *Infect Immun* **76**, 4978–88
1125 (2008).
1126 15. DiGiandomenico, A., Rao, J. & Goldberg, J. B. Oral vaccination of BALB/c mice with
1127 Salmonella enterica serovar Typhimurium expressing Pseudomonas aeruginosa O
1128 antigen promotes increased survival in an acute fatal pneumonia model. *Infect Immun*
1129 **72**, 7012–21 (2004).
1130 16. Bridge, D. R., Whitmire, J. M., Makobongo, M. O. & Merrell, D. S. Heterologous
1131 Pseudomonas aeruginosa O-antigen delivery using a Salmonella enterica serovar
1132 Typhimurium wecA mutant strain. *Int J Med Microbiol* **306**, 529–540 (2016).

1133 17. Zhao, X. *et al.* Recombinant attenuated Salmonella Typhimurium with heterologous
1134 expression of the Salmonella Choleraesuis O-polysaccharide: high immunogenicity
1135 and protection. *Sci Rep* **7**, 7127 (2017).
1136 18. Herrington, D. A. *et al.* Studies in volunteers to evaluate candidate Shigella vaccines:
1137 further experience with a bivalent Salmonella typhi-Shigella sonnei vaccine and
1138 protection conferred by previous Shigella sonnei disease. *Vaccine* **8**, 353–7 (1990).
1139 19. World Health Organization. *WHO Bacterial Priority Pathogens List, 2024: Bacterial*
1140 *Pathogens of Public Health Importance to Guide Research, Development and*
1141 *Strategies to Prevent and Control Antimicrobial Resistance.* (2024).
1142 20. Whitfield, C. & Trent, M. S. Biosynthesis and export of bacterial lipopolysaccharides.
1143 *Annu Rev Biochem* **83**, 99–128 (2014).
1144 21. Vinogradov, E. *et al.* Structures of lipopolysaccharides from Klebsiella pneumoniae.
1145 Eluicidation of the structure of the linkage region between core and polysaccharide O
1146 chain and identification of the residues at the non-reducing termini of the O chains. *J*
1147 *Biol Chem* **277**, 25070–81 (2002).
1148 22. Bronner, D., Clarke, B. R. & Whitfield, C. Identification of an ATP-binding cassette
1149 transport system required for translocation of lipopolysaccharide O-antigen side-
1150 chains across the cytoplasmic membrane of Klebsiella pneumoniae serotype O1. *Mol*
1151 *Microbiol* **14**, 505–19 (1994).
1152 23. Joensen, K. G., Tetzschner, A. M. M., Iguchi, A., Aarestrup, F. M. & Scheutz, F. Rapid
1153 and Easy In Silico Serotyping of Escherichia coli Isolates by Use of Whole-Genome
1154 Sequencing Data. *J Clin Microbiol* **53**, 2410–26 (2015).
1155 24. Choi, K.-H. *et al.* A Tn7-based broad-range bacterial cloning and expression system.
1156 *Nat Methods* **2**, 443–8 (2005).
1157 25. Wong, J. L. C. *et al.* OmpK36-mediated Carbapenem resistance attenuates ST258
1158 Klebsiella pneumoniae in vivo. *Nat Commun* **10**, 3957 (2019).
1159 26. Clements, A. *et al.* Targeting subcapsular antigens for prevention of Klebsiella
1160 pneumoniae infections. *Vaccine* **26**, 5649–53 (2008).
1161 27. Kim, M. *et al.* Bacteria hijack integrin-linked kinase to stabilize focal adhesions and
1162 block cell detachment. *Nature* **459**, 578–82 (2009).
1163 28. Matute-Bello, G. *et al.* An official American Thoracic Society workshop report:
1164 features and measurements of experimental acute lung injury in animals. *Am J Respir*
1165 *Cell Mol Biol* **44**, 725–38 (2011).
1166 29. Osuchowski, M. F. *et al.* Minimum quality threshold in pre-clinical sepsis studies
1167 (MQTiPSS): an international expert consensus initiative for improvement of animal
1168 modeling in sepsis. *Intensive Care Med Exp* **6**, 26 (2018).
1169 30. Schembri, M. A. *et al.* Molecular Characterization of the Multidrug Resistant
1170 Escherichia coli ST131 Clone. *Pathogens* **4**, 422–30 (2015).
1171 31. Lam, M. M. C., Wick, R. R., Judd, L. M., Holt, K. E. & Wyres, K. L. Kaptive 2.0: updated
1172 capsule and lipopolysaccharide locus typing for the Klebsiella pneumoniae species
1173 complex. *Microb Genom* **8**, (2022).
1174 32. Knutton, S. A novel EspA-associated surface organelle of enteropathogenic Escherichia
1175 coli involved in protein translocation into epithelial cells. *EMBO J* **17**, 2166–2176
1176 (1998).
1177 33. Martin, M. J. *et al.* A panel of diverse Klebsiella pneumoniae clinical isolates for
1178 research and development. *Microb Genom* **9**, (2023).

1179 34. Old, D. C. & Adegbola, R. A. A new mannose-resistant haemagglutinin in Klebsiella. *J*
1180 *Appl Bacteriol* **55**, 165–72 (1983).
1181 35. Murphy, C. N. & Clegg, S. Klebsiella pneumoniae and type 3 fimbriae: nosocomial
1182 infection, regulation and biofilm formation. *Future Microbiol* **7**, 991–1002 (2012).
1183 36. Yang, J. *et al.* Transcriptional activation of the mrkA promoter of the Klebsiella
1184 pneumoniae type 3 fimbrial operon by the c-di-GMP-dependent MrkH protein. *PLoS*
1185 *One* **8**, e79038 (2013).
1186 37. Ma, C. *et al.* Citrobacter rodentium infection causes both mitochondrial dysfunction
1187 and intestinal epithelial barrier disruption in vivo: role of mitochondrial associated
1188 protein (Map). *Cell Microbiol* **8**, 1669–86 (2006).
1189 38. Leverton, L. Q. & Kaper, J. B. Temporal expression of enteropathogenic Escherichia coli
1190 virulence genes in an in vitro model of infection. *Infect Immun* **73**, 1034–43 (2005).
1191 39. Riechmann, L., Clark, M., Waldmann, H. & Winter, G. Reshaping human antibodies for
1192 therapy. *Nature* **332**, 323–7 (1988).
1193 40. Lee, E.-C. *et al.* Complete humanization of the mouse immunoglobulin loci enables
1194 efficient therapeutic antibody discovery. *Nat Biotechnol* **32**, 356–63 (2014).
1195 41. Feldman, M. F. *et al.* A promising bioconjugate vaccine against hypervirulent Klebsiella
1196 pneumoniae. *Proc Natl Acad Sci U S A* **116**, 18655–18663 (2019).
1197 42. Walker, K. A., Treat, L. P., Sepúlveda, V. E. & Miller, V. L. The Small Protein RmpD Drives
1198 Hypermucoviscosity in Klebsiella pneumoniae. *mBio* **11**, (2020).
1199 43. Mavridou, D. A. I., Gonzalez, D., Clements, A. & Foster, K. R. The pUltra plasmid series:
1200 A robust and flexible tool for fluorescent labeling of Enterobacteria. *Plasmid* **87–88**,
1201 65–71 (2016).
1202 44. Hopkins, E. G. D., Roumeliotis, T. I., Mullineaux-Sanders, C., Choudhary, J. S. & Frankel,
1203 G. Intestinal Epithelial Cells and the Microbiome Undergo Swift Reprogramming at the
1204 Inception of Colonic Citrobacter rodentium Infection. *mBio* **10**, (2019).
1205

FIGURE 1.

A.

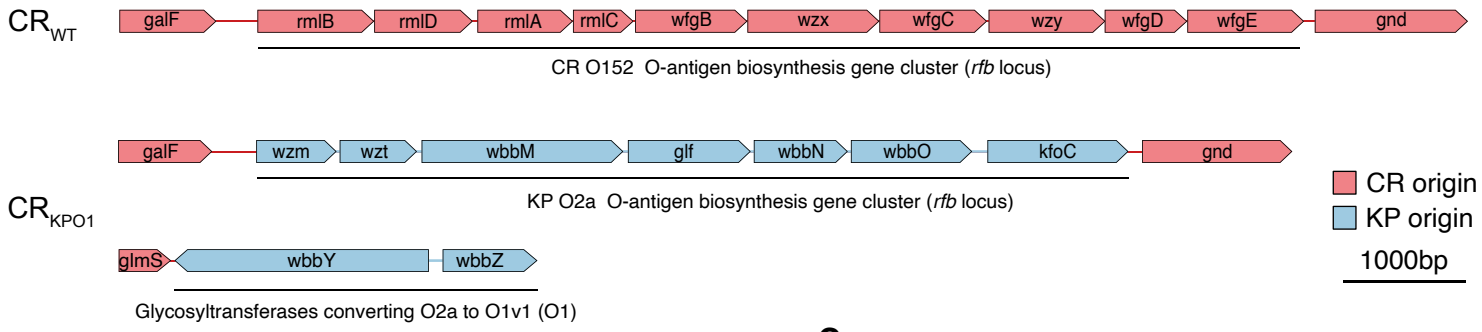

B.

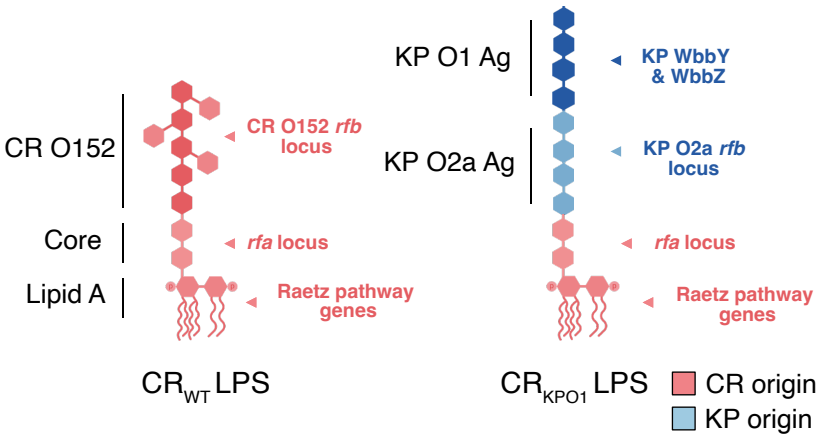

C.

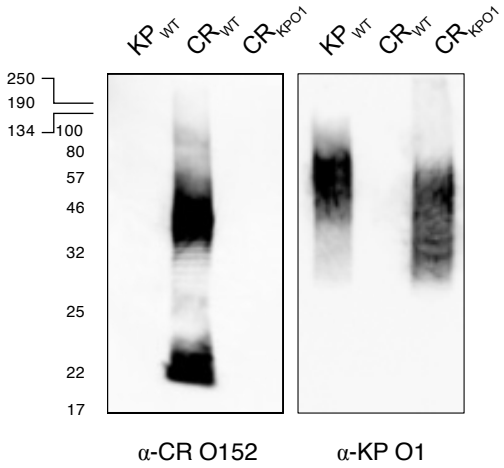

D.

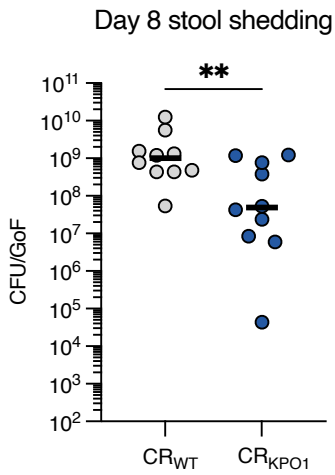

E.

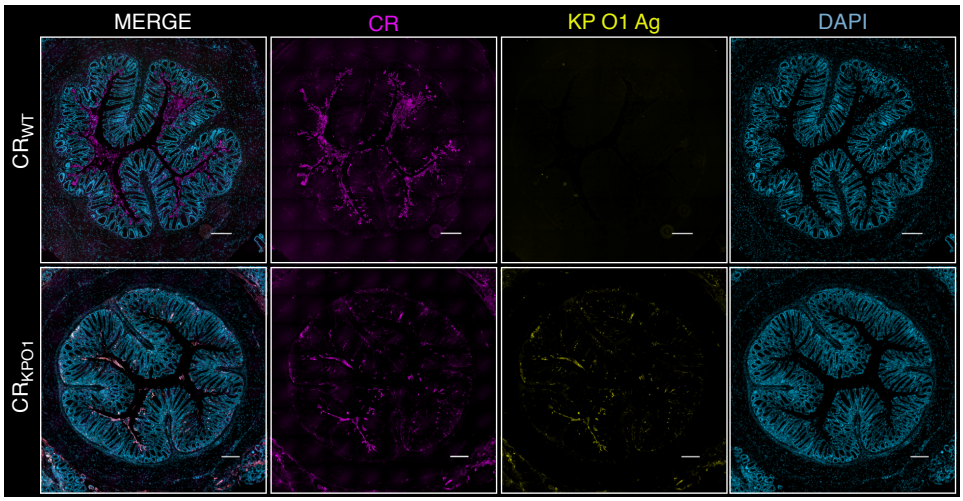

FIGURE 2.

A.

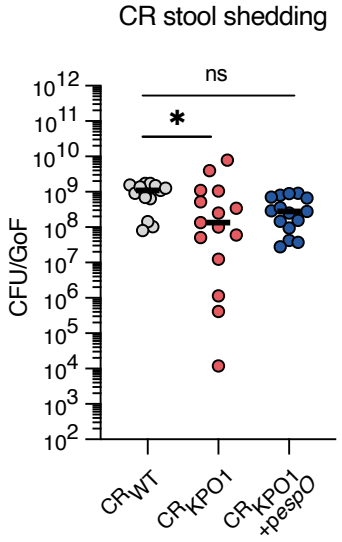

B.

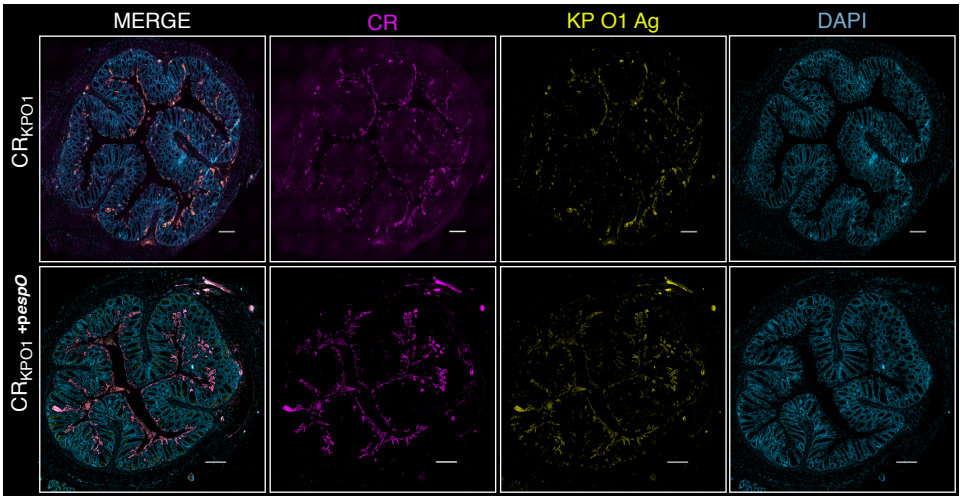

C.

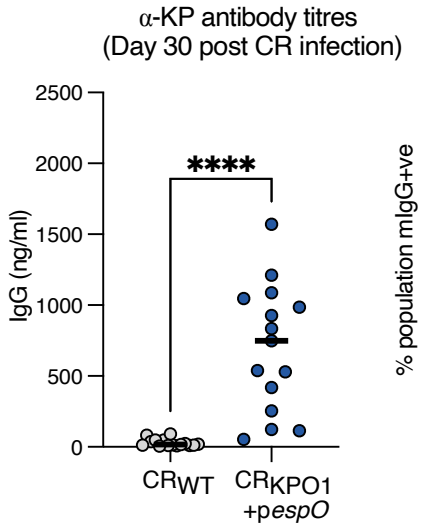

D.

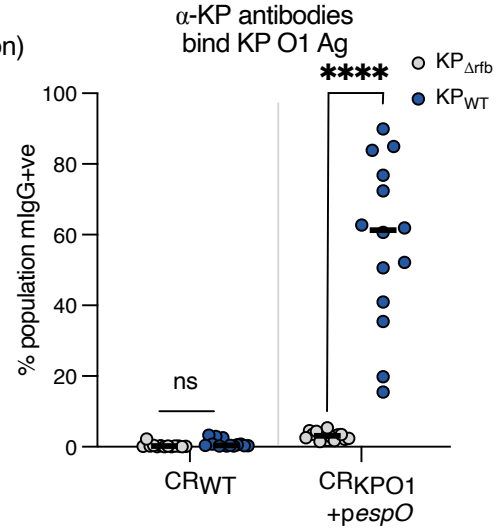

E.

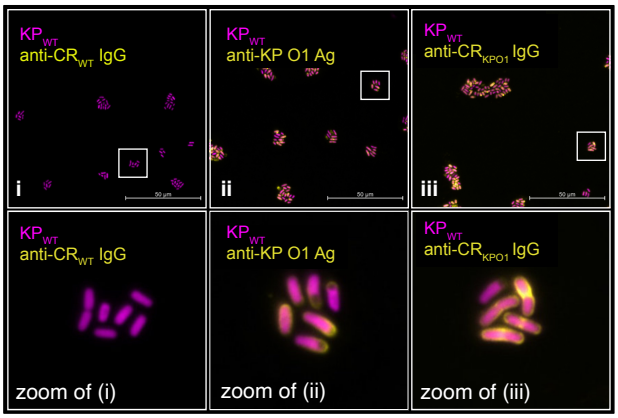

FIGURE 3.

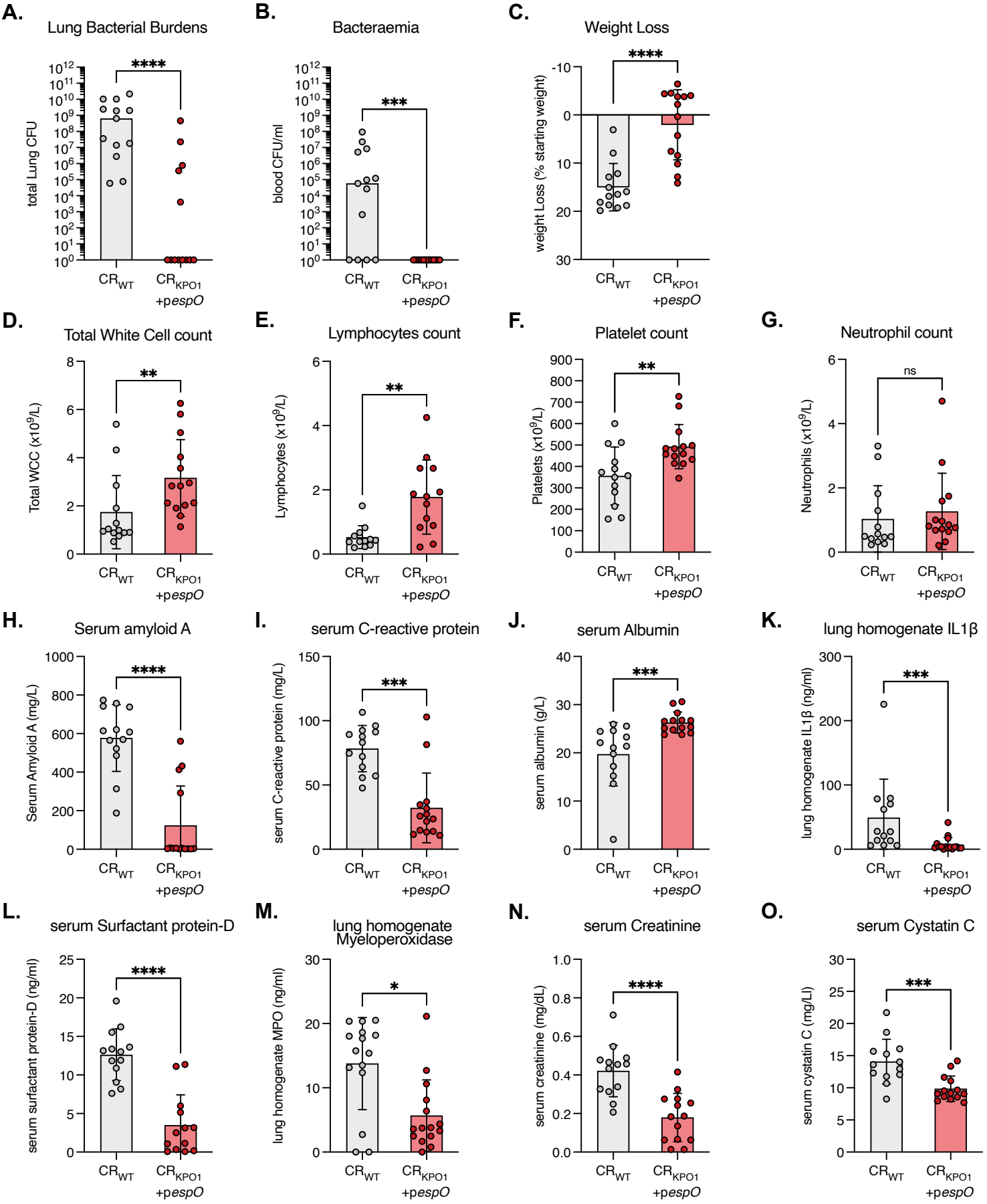
A.
Lung Bacterial Burdens
total Lung CFU
****
B.
Bacteraemia
blood CFU/ml
***
C.
Weight Loss
weight Loss (% starting weight)
****
D.
Total White Cell count
Total WCC (x10⁹/L)
**
E.
Lymphocytes count
Lymphocytes (x10⁹/L)
**
F.
Platelet count
Platelets (x10⁹/L)
**
G.
Neutrophil count
Neutrophils (x10⁹/L)
ns
H.
Serum amyloid A
Serum Amyloid A (mg/L)
****
I.
serum C-reactive protein
serum C-reactive protein (mg/L)
***
J.
serum Albumin
serum albumin (g/L)
***
K.
lung homogenate IL1β
lung homogenate IL1β (ng/ml)
***
L.
serum Surfactant protein-D
serum surfactant protein-D (ng/ml)
****
M.
lung homogenate Myeloperoxidase
lung homogenate MPO (ng/ml)
*
N.
serum Creatinine
serum creatinine (mg/dL)
****
O.
serum Cystatin C
serum cystatin C (mg/Ll)
***
CR_WT
CR_KPO1 +pespO

FIGURE 4.

A.

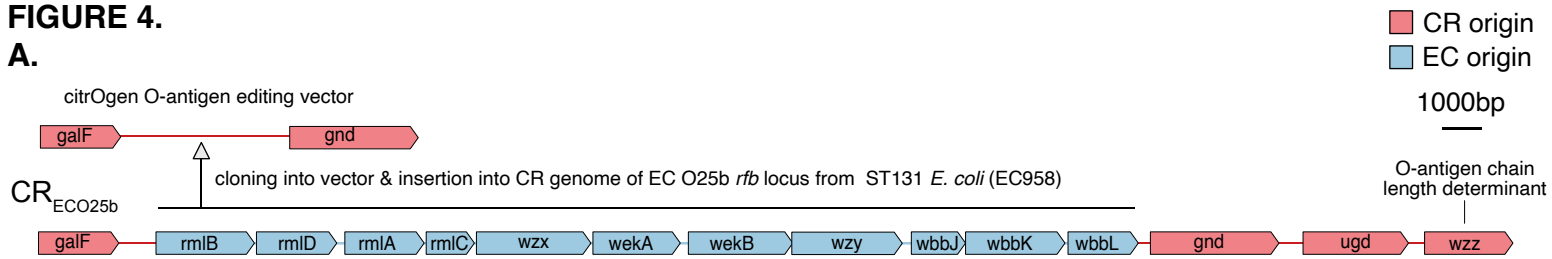

B.

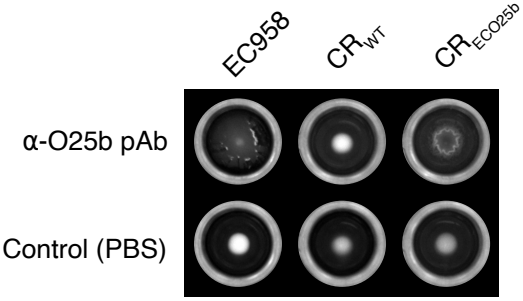

C.

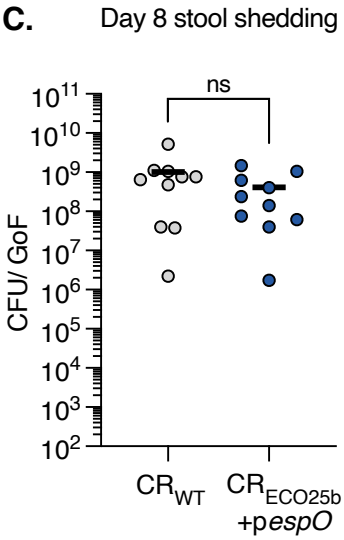

D.

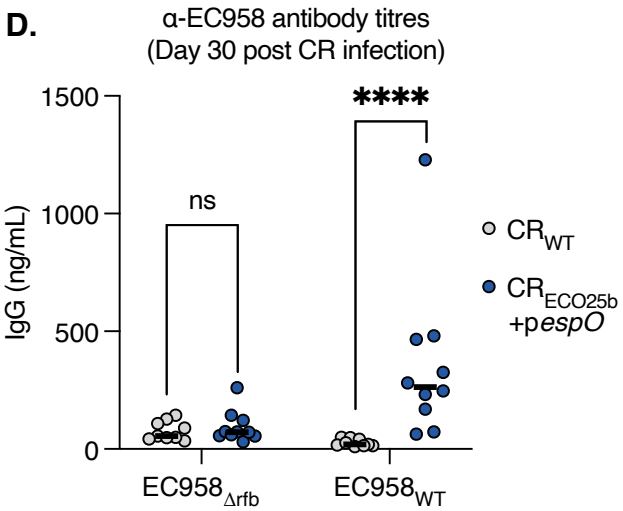

FIGURE 5.

A.

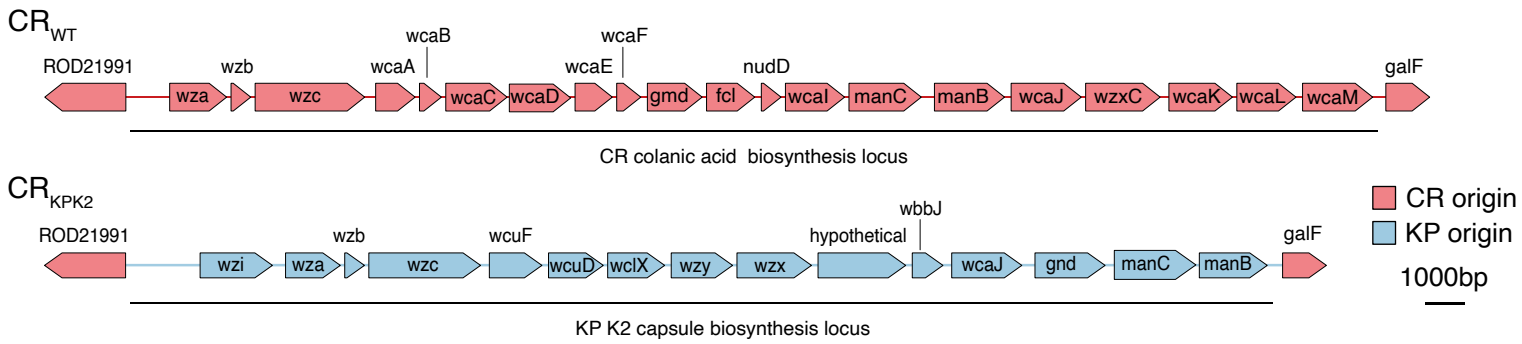

B.

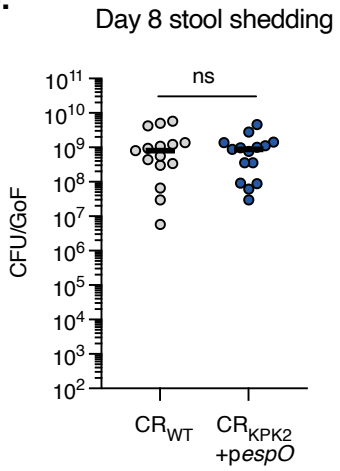

C.

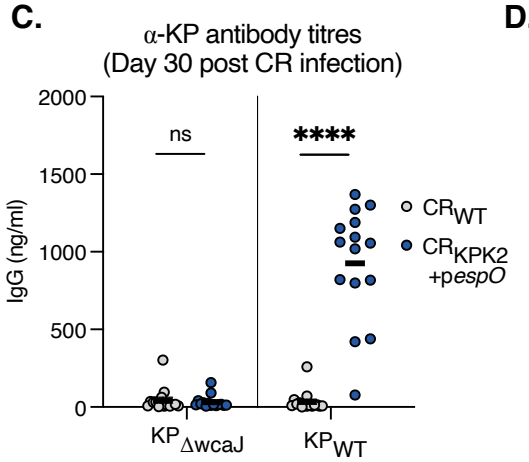

D.

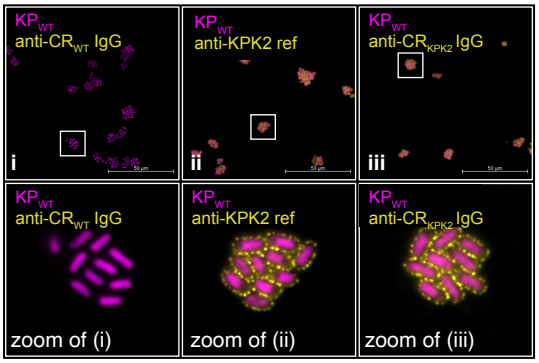

E.

KL25	KL31	KL38	KL38	KL148	KL30	KL62	KL17	KL3	KL25
KL23	KL10	KL3	KL17	KL142	KL60	KL62	KL113	KL42	KL63
KL2	KL14	KL28	KL24	KL28	KL105	KL151	KL102	KL30	KL52
KL19	KL30	KL119	KL110	KL3	KL154	KL146	KL27	KL15	KL125
KL51	KL64	KL2	KL52	KL57	KL5	KL3	KL25	KL51	KL57
KL21	KL107	KL15	KL113	KL58	KL51	KL10	KL2	KL30	KL1
KL43	KL30	KL64	KL61	KL27	KL9	KL46	KL36	KL116	KL62
KL2	KL35	KL20	KL28	KL13	KL61	KL2	KL51	KL112	KL14
KL102	KL62	KL39	KL30	KL46	KL15	KL14	KL65	KL54	KL107
KL122	KL46	KL15	KL2	KL2	KL128	KL62	KL107	KL64	KL107

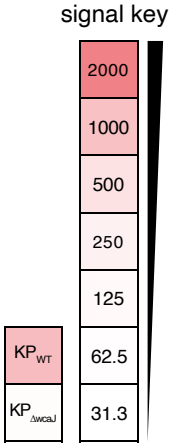

F.

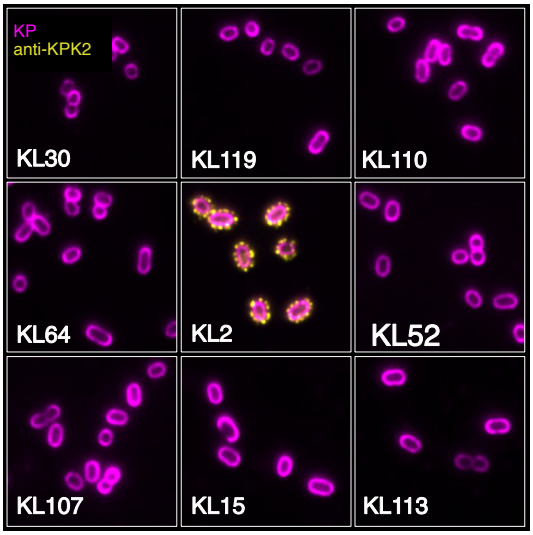

FIGURE 6.

A.

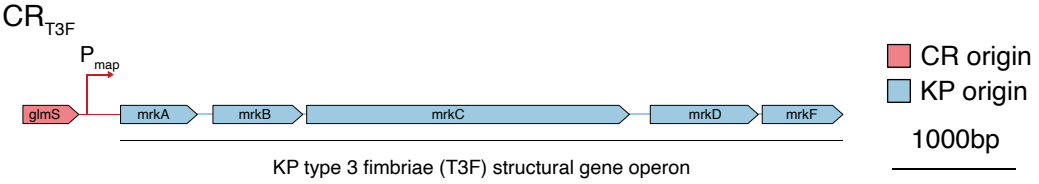

B.

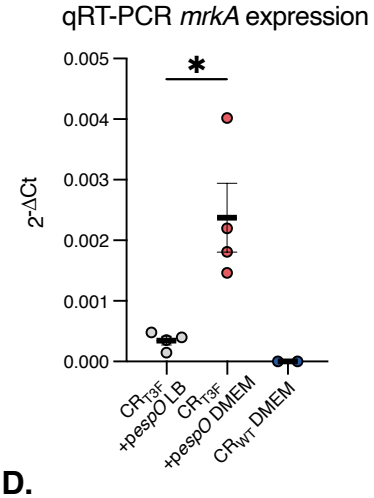

C.

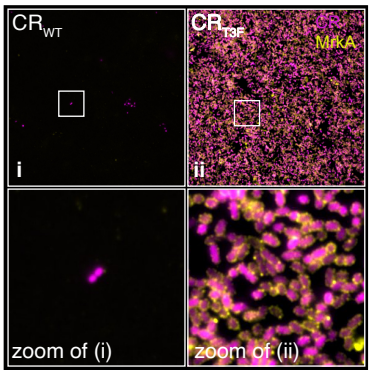

D.

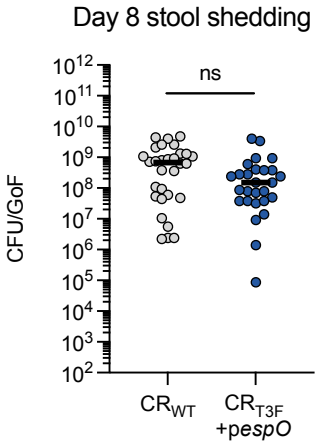

E.

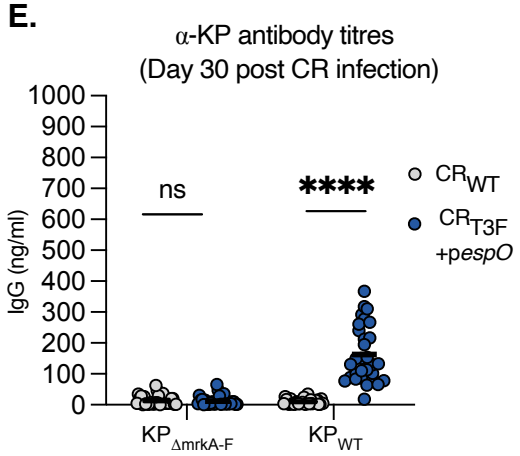

F.

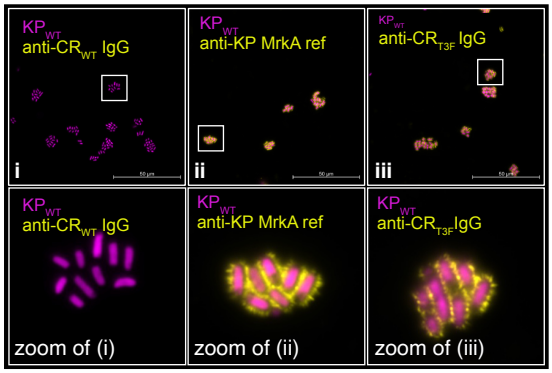

G.

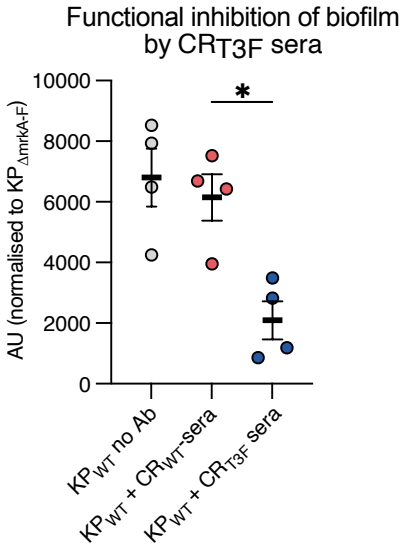

H.

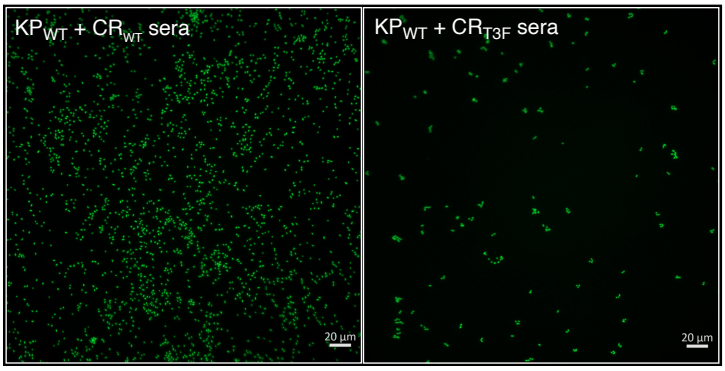

FIGURE 7.

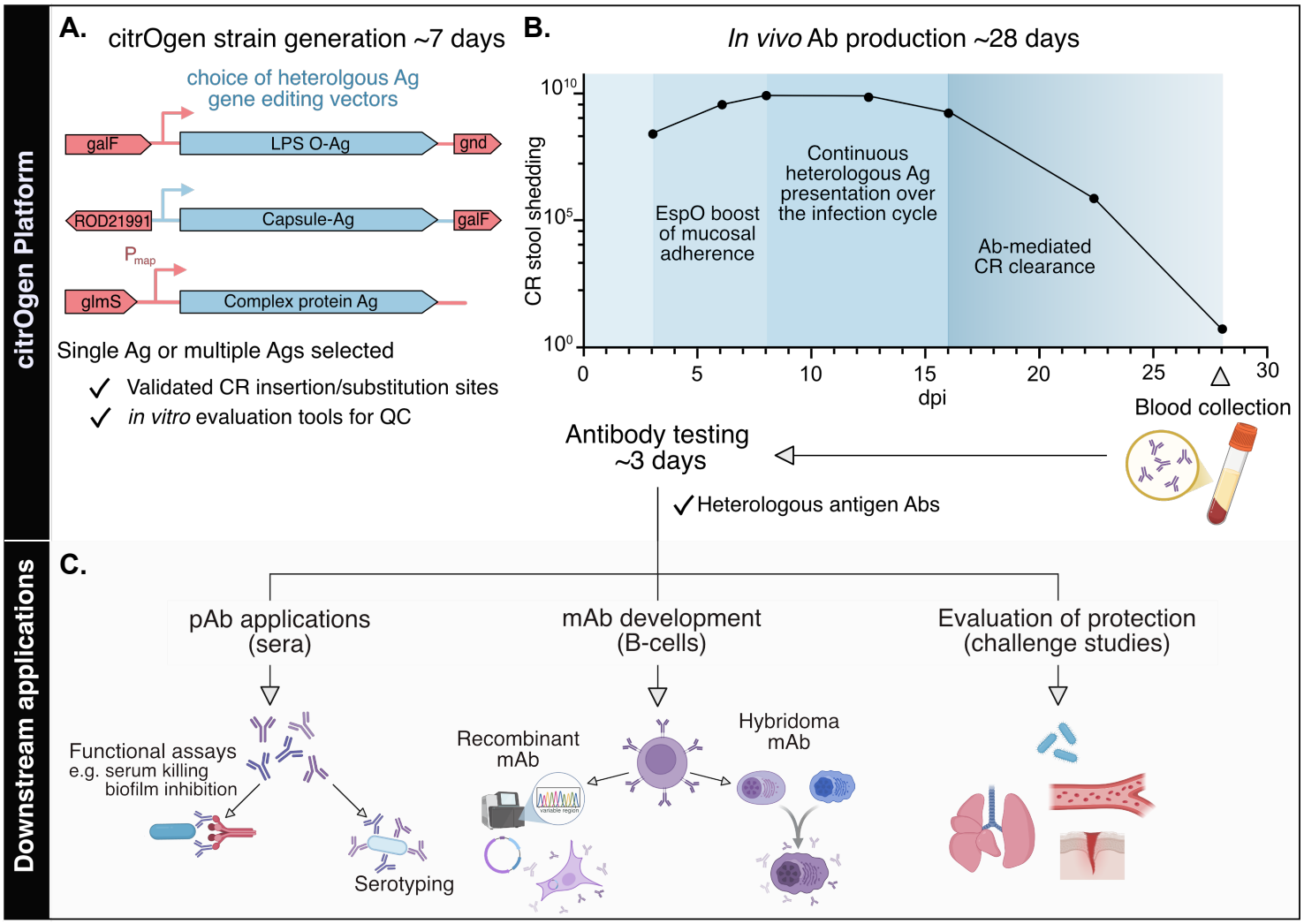
citrOgen Platform
A.
citrOgen strain generation ~7 days
choice of heterolgous Ag gene editing vectors
galF
LPS O-Ag
gnd
ROD21991
Capsule-Ag
galF
Pmap
glmS
Complex protein Ag
Single Ag or multiple Ags selected
✓ Validated CR insertion/substitution sites
✓ in vitro evaluation tools for QC
B.
In vivo Ab production ~28 days
CR stool shedding
10¹⁰
10⁵
10⁰
EspO boost of mucosal adherence
Continuous heterologous Ag presentation over the infection cycle
Ab-mediated CR clearance
0
5
10
15
20
25
30
dpi
Blood collection
Antibody testing ~3 days
✓ Heterologous antigen Abs
Downstream applications
C.
pAb applications (sera)
mAb development (B-cells)
Evaluation of protection (challenge studies)
Functional assays e.g. serum killing biofilm inhibition
Serotyping
Recombinant mAb
Hybridoma mAb